Sex- and Diet- Dependent Microglial and Proteomic Responses to Chronic Diesel Exhaust Exposure in the *Ldlr*$^{-/-}$ Mouse Brain

Jenielle Guevarra Domaoal

A thesis

submitted in partial fulfillment of the

requirements for the degree of

Master of Science

University of Washington

2026

Committee:

Judit Marsillach

Katherine E. Prater

Program Authorized to Offer Degree:

Department of Environmental and Occupational Health Sciences

University of Washington

Abstract

Sex- and Diet- Dependent Microglial and Proteomic Responses to Chronic Diesel Exhaust Exposure in the *Ldlr*$^{-/-}$ Mouse Brain

Jenielle Guevarra Domaoal

Chair of the Supervisory Committee:

Judit Marsillach

Department of Environmental and Occupational Health Sciences

Background: Air pollution is one of the leading causes of mortality, contributing to about 6.7 million premature deaths annually. Diesel exhaust (DE) is a significant contributor to particulate matter (PM) in urban traffic-related air pollution, resulting in adverse respiratory, cardiovascular, and reproductive health effects. Research has suggested that PM can also affect the brain and central nervous system, triggering neurodegeneration. Microglia, the brain's resident immune cells, play a crucial role in regulating PM-induced toxicity. To protect the brain from damage, resting microglia are activated to eliminate foreign substances and dead cells, while initiating an inflammatory response. Though initially beneficial to maintain homeostasis and repair damage, prolonged exposure to PM can cause microglia to promote a pro-inflammatory environment due to oxidative stress and cell death, leading to disease escalation. Vulnerable and susceptible populations have an increased risk of PM-induced toxicity. People with genetic mutations, like familial hypercholesterolemia (FH), are at an increased risk of neurodegenerative disease due to their increased risk of cardiovascular disease. While there is increasing research to uncover how PM impacts neurodegeneration, the specific molecular mechanisms are not well understood. The

objective of this project was to characterize the effects of chronic DE exposure and a high-fat diet on neuroinflammatory and proteomic responses in the hippocampus and olfactory bulb of a mouse model of FH. Based on publications and our laboratory's preliminary data, we hypothesize that chronic DE exposure will induce sex-specific changes in microglial states and protein pathways, particularly in the hippocampus and olfactory bulb, and that these changes will be exacerbated by HFD in hypercholesterolemic mice.

Methods: This study examined mechanisms of PM-induced neuroinflammation and cognitive dysfunction, focusing on proteomics and microglia. Six-week-old *low-density lipoprotein receptor knockout* (*Ldlr*$^{-/-}$) mice, a model of FH, were exposed to freshly generated DE (~250 μg/m^3) or filtered air (FA) over 18 weeks. Mice (n=11-13 per sex and exposure) were fed a high-fat (HFD) or chow diet and exposed for 6 h/day, 5 days/week. At the end of 18 weeks, mice were sacrificed and perfused with PBS. Left brain hemispheres were fixed, cryopreserved, and used for immunofluorescence. Confocal images (40x) were taken for each group (n = 2), and an average cell count was taken. From each 40x image, a 3x zoom image was taken, and soma and arborization area were measured for 3 random microglia. The hippocampus and olfactory bulb were isolated from right brain hemispheres, flash frozen in liquid nitrogen, analyzed for proteomics via data-independent acquisition liquid chromatography-tandem mass spectrometry (DIA LC-MS/MS). Resulting datasets were analyzed using the Advaita iPathwayGuide software.

Results: An overall decrease in microglia was found in the DE groups when compared to the FA groups, highlighting possible microglial dysfunction based on diet and DE exposure. The HFD DE female (DEF) group had the largest decrease ($p= 0.0463$) in microglial cell count (42%) and the largest increase in soma (~19%) and arborization area (~66%). Protein analysis revealed significant changes (FDR< 0.05) based on exposure (FA or DE) in the olfactory bulb between the HFD DE and HFD FA female groups. In the hippocampus and olfactory bulb of male mice, protein changes observed were based on diet when comparing HFD DE and control chow DE groups

and the HFD FA and control chow FA groups. Pathway analysis of the hippocampus identified dysregulation of the actin cytoskeleton pathway in the HFD FA male group, which is associated with synaptic dysfunction and possible cognitive decline. In the olfactory bulb, the pathway analysis also revealed impacts on glutamate synapses in the HFD DEF, which is also associated with synaptic dysfunction.

Conclusion: Overall, the preliminary findings in this project suggest that chronic DE exposure and HFD alter microglial morphology and abundance in a sex-dependent manner, with significant protein changes in pathways relevant to neurodegenerative processes. Additional research is underway and needed to ascertain whether DE-induced microglial states overlap with microglial signatures implicated in Alzheimer's disease and other neurodegenerative conditions, which could provide a mechanistic insight into how air pollution contributes to neurodegenerative disease risk.

Table of Contents

List of Abbreviations

Abbreviations	Definitions
AD	Alzheimer’s disease
ADRD	Alzheimer's disease and related dementias
CA1	Cornu ammonis 1
CA3	Cornu ammonis 3
CNS	Central nervous system
DE	Diesel exhaust
DEF	Diesel exhaust female
DEM	Diesel exhaust male
DG	Dentate gyrus
DPF	Diesel particulate filter
DPM	Diesel particulate matter
FA	Filtered air
FAF	Filtered air female
FAM	Filtered air male
HFD	High-fat diet
Iba1	Ionized calcium-binding adapter molecule 1
IF	Immunofluorescence
LDL	Low-density lipoprotein
LDLR	*Low-density lipoprotein receptor* (gene)
Ldlr -/-	Low-density lipoprotein receptor knockout
MASH	Metabolic dysfunction-associated steatohepatitis
NLD	Northlake Diesel facility
PAHs	Polycyclic aromatic hydrocarbons
PM	Particulate matter
ROS	Reactive oxygen species
SVOC	Semi-volatile organic compounds
UFP	Ultrafine particulate matter

List of Figures

In the olfactory bulb when comparing the (B) HFD FAF and HFD DEF groups, the most significant pathway was related to glutamatergic synapses.

Supplementary Figure 1. Pathway analysis bubble plots did not yield significant results in the olfactory bulb when comparing between the (A) HFD FAM and chow FAM groups and the (B) HFD FAF and HFD DEF groups.

Supplementary Table 2. Resulting F and P-values ($\alpha = 0.05$) from comparisons between all main effects, comparisons between male groups, and comparisons between HFD groups. The Adjusted p-values are also listed for comparisons that were trending ($p = 0.05$) or significant ($p < 0.05$).

List of Tables

Acknowledgements

I would like to thank my committee, Dr. Judit Marsillach and Dr. Katherine E. Prater, for their guidance and support as I completed this project. Attempting to complete a master's thesis within 2 years is tough, and I don't think I would have been able to succeed if it wasn't for the unwavering support and confidence in me. Thank you to the members of the Marsillach lab for sharing my grief in the lab when experiments didn't go as planned and for continuing to cheer me on.

I would like to thank my friends for telling me to bet on myself and my family for being the inspiration I needed to do it. Thank you for all the times you had to listen to me complain about how hard it was to be a master's student, and for encouraging me to keep going. My cup has been continuously filled because of all your help. I will always be eternally grateful for my community.

This work was supported by the National Institute of Environmental Health Sciences (NIEHS R01 ES033703-01) & Admin Supplemental UW RRF(#A222295), the UW EDGE Career Development Investigator (P30 ES007033), and the DEOHS Sheldon D. Murphy Endowment.

Background

1. Air Pollution, Traffic Related Particulate Matter, and Diesel Particulate Matter

Anthropogenic (human-caused) air pollution is a global public health issue, with about 140 million people in the US alone living in areas with pollution levels above the primary National Ambient Air Quality Standards (US Environmental Protection Agency, 2024a). According to the State of Global Air Report (2025), 7.9 million deaths in 2023 were credited to air pollution (**Fig.1.**), making it the second ranked cause of death globally (Health Effects Institute, 2025). Emission sources of air pollution are split into 4 major categories: major, area, mobile, and natural sources. Mobile sources (vehicles), or traffic-related air pollution, constitute around 80% of air pollution and contains exhaust related emissions (elemental and organic carbon and elements from the incomplete combustion of fuel) and non-exhaust emissions (particles from brake wear, tire wear, engines, and tire friction with roads) (Manisalidis et al., 2020; Matthaios et al., 2022).

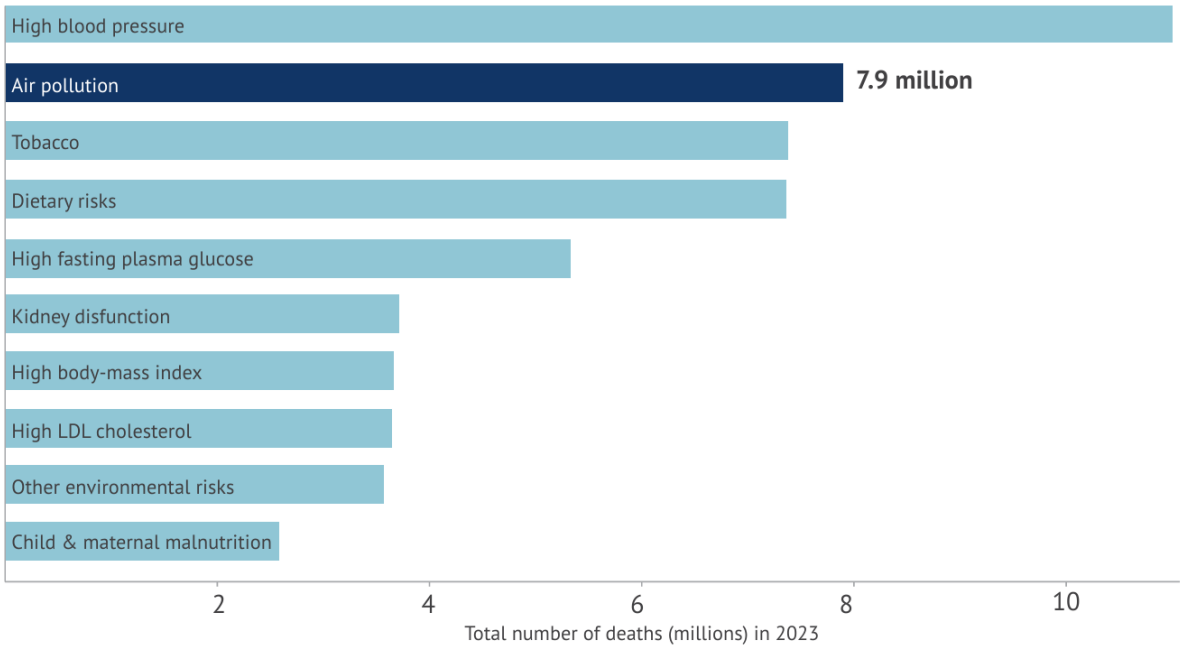

Figure 1. Total number of deaths in 2023, globally ranked by risk factors. Figure reprinted from the State of Global Air Report, 2025.

Exhaust emissions, such as those from diesel engines, generate particulate matter (PM) due to the incomplete combustion of fuel (Gerber et al., 2024), which is a significant risk factor to global mortality. Of the 7.9 million deaths attributed to air pollution in 2023, 4.9 were credited to fine particulate matter ($PM_{2.5}$) exposure (Health Effects Institute, 2025). Particulate matter (PM) is a complex mixture of solids and aerosols derived from different emission sources. PM is categorized based on their aerodynamic diameter (**Fig.2.**) into coarse (PM_{10}, < 10 μm is diameter), fine ($PM_{2.5}$, < 2.5 μm in diameter), or ultrafine (UFP, $PM_{0.1}$, < 0.1 in diameter) (Landwehr et al., 2021). Among the sources of exhaust emissions, diesel exhaust (DE) is one of the major generators of UFP.

UFPs contribute greatly to the particle number count in ambient (outdoor) air in urban areas with traffic (Damayanti et al., 2023) and are linked to several adverse health effects due to their ability to be inhaled and deeply deposit into the lower respiratory tract. These particles can cross the air-blood barrier, and enter systemic circulation, affecting distal organs. UFPs are also more likely to accumulate in the olfactory epithelium and bypass the blood-brain barrier through the olfactory nerve, entering and potentially impacting the brain (Balachandar et al., 2025; Gerber et al., 2024). Due to the large surface-area-to-mass ratio, UFP can also carry a considerable amount of adsorbed material per unit mass, which can include volatile organic compounds, ketones, and heavy metals (Landwehr et al., 2021; Schraufnagel, 2020), further increasing risk of toxicity and development of adverse health effects.

Three parts, a liquid phase, gaseous phase, and solid phase, make up DE related emissions. Carbon monoxide, nitrogen oxides, hydrocarbons, and polycyclic aromatic hydrocarbons (PAHs), among others, make up the gaseous phase (**Fig.2.**). The solid phase is made up of carbonaceous soot particles, metals and their oxides, while the liquid phase consists of nitrates, sulfates, and adsorbed PAHs, with their nitro- and oxygenated derivatives. Diesel particulate

matter (DPM) is formed from the solid and liquid fragments of diesel emissions (Tsakonas et al., 2025).

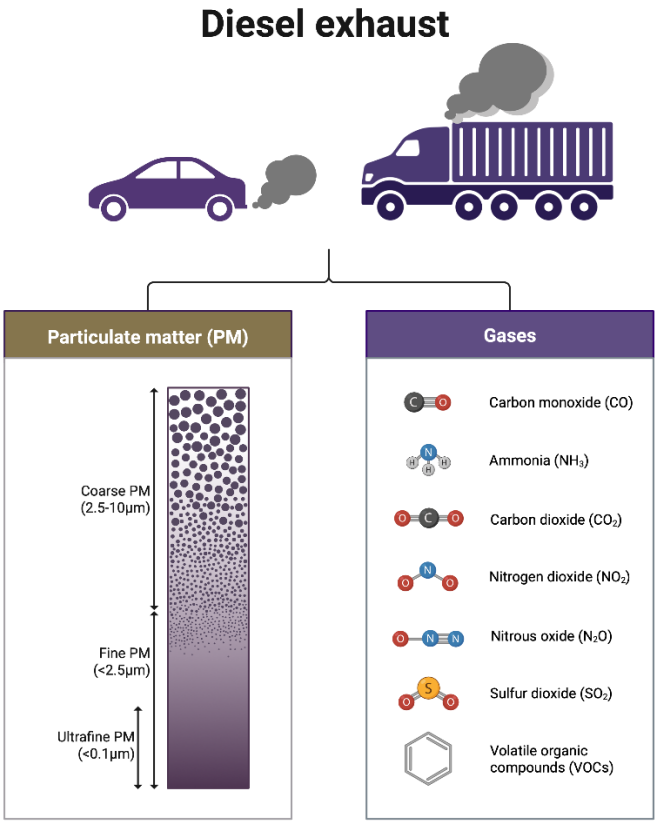

Figure 2. Characterization of diesel particulate matter (DPM) size and some of the chemicals within diesel exhaust. Figure made with BioRender.com.

UFP can also be categorized by particle number size distributions which include nucleation (<25 nm), Aitken (25-100 nm) and Accumulation (100-1000 nm) modes. Nucleation mode particles are comprised of semi-volatile organic and sulfur compounds. During the exhaust dilution process when gas exits the tailpipe, these compounds nucleate to form liquid nanoparticles (UFP, < 50 nm in diameter). Nucleation mode particles can contribute to around 90% of particle numbers (Vaaraslahti et al., 2004). While current diesel engines are equipped with aftertreatment technologies, like diesel particulate filters (DPFs), that reduce overall UFP and other criteria

emissions, current technology is insufficient at consistently keeping UFP emissions below regulation limits. To maintain efficient function, DPFs must undergo periodic regeneration, where soot buildup is burned and removed. During this process, particle number increases close to levels released by vehicles without DPFs. DPFs are effective at capturing larger particles; however, they are less effective at controlling UFP and secondary UFP that form in the atmosphere, particularly nucleation mode (particle diameter, d_p<30nm) particle emissions, and may exceed regulations during regeneration. (Damayanti et al., 2023; Ma et al., 2025; Tsakonas et al., 2025). Aftertreatment technology may reduce UFP emissions overall, but their abilities seem to be limited.

2. Diesel Exhaust Exposure

DE can harbor hundreds of chemicals creating a toxic cocktail of different components that, combined, are known to cause severe respiratory and cardiovascular system effects (Landwehr et al., 2021). DE is even classified as a group 1 carcinogen (sufficient evidence of carcinogenicity to humans) (IARC, 2012). While DE gases are associated with adverse health outcomes, DPM is often considered the major promoter of detrimental health effects within DE (Weitekamp et al., 2020).

There are two proposed pathways of how PM can enter the body to inflict possible damage. The indirect pathway is through translocation from the respiratory tract into circulation. Smaller particles, like $PM_{2.5}$ and UFP, are inhaled and deposited deep into the lungs, triggering an immune response. Larger $PM_{2.5}$ particles can be caught by the macrophages and phagocytosed, while UFP can evade detection and cross the alveoli into systemic circulation, triggering an inflammatory response and possibly reaching other organs to cause additional damage (Singh & Sharma, 2025). Particles can disrupt the integrity of the blood-brain barrier and cross it, accessing the brain directly (O'Piela et al., 2022). The secondary proposed pathway is more direct and specific to the brain. As UFP are inhaled and enter the nose, they can translocate through the

olfactory nerve to the olfactory bulb, or via the trigeminal nerve in the nasal vestibule and cavity, potentially impairing olfactory function (Ajmani, Suh, & Pinto, 2016). DPM exposure can cause increased oxidative stress, with reactive oxygen species (ROS) triggering subsequent molecular and cellular reactions that lead to an inflammatory and immune response. Continuous PM exposure influences this interaction between oxidative stress, innate and adaptive immune activation, and chronic inflammation, resulting in chronic respiratory outcomes (asthma, COPD), cardiovascular conditions (Bradley et al., 2013; Miller & Newby, 2020), and a compromised immune system (Singh & Sharma, 2025). In a study that exposed 9-week-old male Sprague-Dawley rats to DPM (0.2 mg/ml) for 20 min/day for 5 weeks, researchers found cardiac dysfunction. Additional studies also found increased respiratory inflammation in non-asthmatic mice and increased respiratory inflammation and oxidative stress in asthmatic mice (200 $\mu g/m^3$ for 7 weeks or 169 $\mu g/m^3$ for 8 weeks) (Tanaka et al., 2013), and negative changes in atherosclerotic plaques in ApoE ko mice (200 $\mu g/m^3$, 7 weeks) (Bai et al., 2011; Landwehr et al., 2021). An increasing number of studies are focusing on the link between DE and its effect on the central nervous system (CNS) and neurodegeneration (**Fig.3.**) as onset and progression of CNS related diseases and dementias (Alzheimer's disease and Parkinson's disease) have been associated to PM exposure in epidemiological studies (Barnhill et al., 2020; Jones et al., 2025; Zhao et al., 2026).

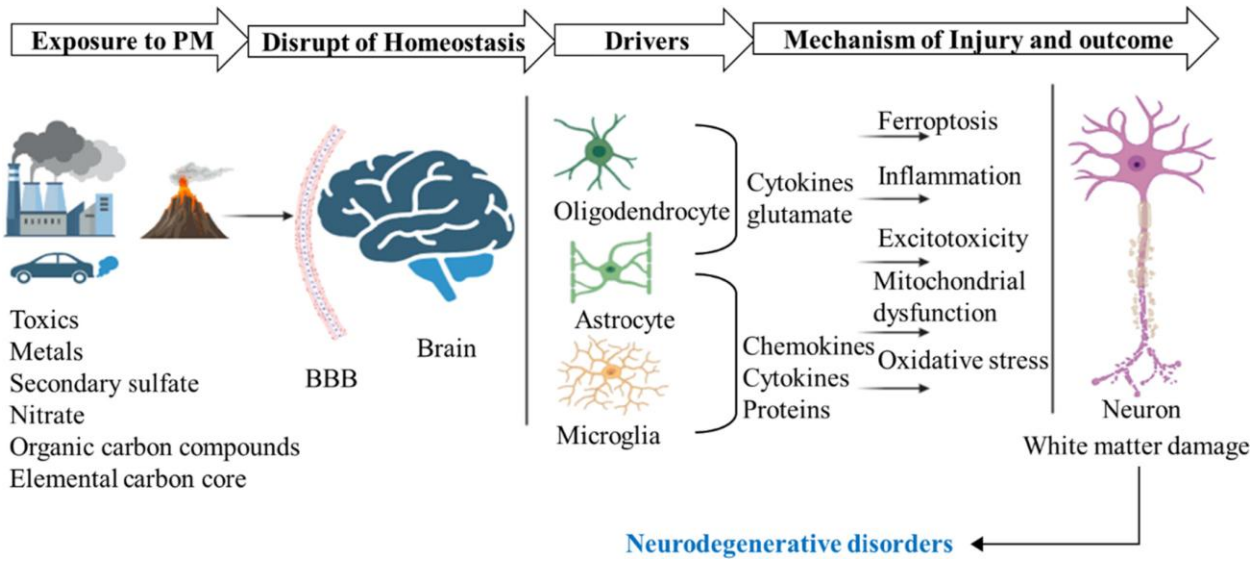

Figure 3. Flow diagram from (Thangavel et al., 2025) showing the mechanistic pathway leading to neuronal death after PM exposure. PM crosses the blood-brain-barrier through the systemic circulation, leading to activation of glial cells, which trigger an immune and inflammatory response. Glial cells become dysfunctional with continued PM exposure, ultimately leading to neuronal damage and neurodegenerative disorders.

3. Neurodegeneration and the Role of Microglia

Neurodegeneration is characterized by neuronal dysfunction and death, and, in some cases, the buildup of altered proteins in the brain (Lamptey et al., 2022). Neurons are nerve cells found in the brain and body that are responsible for sending and receiving signals, which is imperative for how we think, feel, and act (NIH, 2019). While there is a fraction of neurons that can be regenerated, irreparable neuronal death is key to the progression of neurodegenerative disease. While earlier studies have highlighted the impact of genetic factors on neurodegenerative disease progression, current research has highlighted that environmental determinants, like PM, also contribute equally to neurodegenerative disease risk (Lamptey et al., 2022). As seen in neurodegenerative diseases, similar key pathophysiological events, including inflammation, oxidative stress, microglial activation, and neuronal death, are observed in response to PM, stressing a similar pathway of disease progression (Ehsanifar et al., 2022; Hajipour et al., 2020).

Research has worked to uncover how PM contributes to neurodegeneration; however, the specific molecular mechanisms are still not well understood. The hippocampus is crucial for learning and memory and is incredibly vulnerable to damage, inflammation, and atrophy. This gives it an essential part in neurodegenerative diseases, like Alzheimer's disease (Anand & Dhikav, 2012; Mueller et al., 2010). When exposed to DE, memory and behavior in mice is altered, and neurogenesis is impaired (Ehsanifar et al., 2023; Li et al., 2020). Additional animal studies have also found evidence of neurological effects when animals were exposed to DE. Studies in male mice, exposed to DE concentrations between 100 $\mu g/m^3$ – 300 $\mu g/m^3$, found impaired neurogenesis (250 $\mu g/m^3$ for less than a day), increased neuroinflammation (173 and 149 $\mu g/m^3$, 4 weeks), and an impact on object recognition ability (129 $\mu g/m^3$, 12 week) (Landwehr et al., 2021). In a study using a zebrafish model, researchers found behavioral deficits and a significant decrease in neuron number when exposed to DPM extracts (10-25 µg/ml, 24 hr) (Barnhill et al., 2020).

Research on the extent of microglia activation in PM-induced neurodegeneration has grown substantially in recent years. Microglia are the main innate immune cells in the brain and are thought to be key regulators of PM-induced toxicity (Costa et al., 2020; Song et al., 2022; Song et al., 2026). To protect the CNS from damage, microglia continuously survey their environment and adopt different states in response to it, commonly referred to microglial activation. They are responsible for phagocytosis and elimination of misfolded proteins, cellular debris, and dying cells, as well as particles, including PM (Roqué et al., 2016) and trigger an inflammatory response, among other roles. This inflammatory response is initially beneficial as it helps maintain homeostasis and repair damage, but continued neuroinflammation can lead to disease. In the case of AD, early and continued activation of microglia may be involved in the initiation and progression of the disease, with pro-inflammatory microglia affecting the homeostatic function of all brain cells in a deleterious way (Saitgareeva et al., 2020b).

Previous research has aimed to identify changes in the number of microglia in response to DE through staining with ionized calcium-binding adapter molecule 1 (Iba1), a common protein marker used to assess microglia and macrophage quantity in the brain. Multiple *in vivo* studies showed an increase in Iba1 in response to DE exposure, highlighting possible microglial proliferation in response to DE (Cole et al., 2016; Li et al., 2020; Shkirkova et al., 2022). Other studies have used different techniques, like omics (Gao et al., 2022; Ng et al., 2023; Prater et al., 2023), to determine the molecular mechanisms of microglia in neuroinflammation and neurodegeneration, but there are limited studies looking at the impact of sex, diet, and chronic DE exposure on molecular microglial changes. In a study that exposed 7-week old male mice to DPM (300-350 $\mu g/m^3$) for 6 h per day, 5 days per week, for 6 or 12 weeks, researchers found an increase in microglia in the dentate gyrus (DG) and cornu ammonis 1 (CA1) regions of the hippocampus and an increase of mRNA expression for inflammatory cytokines, IL-8, IL1α, IL-1β, IL-6, and TNF-α (Ehsanifar et al., 2023). This study conveys the effect of chronic DE exposure on male mouse brains and its potential to affect microglia related activity. In another study, researchers tested the effects of nanoparticle-rich DE at two doses, a middle dose, 47 $\mu g/m^3$, and a high dose, 129 $\mu g/m^3$, for 3 months on female BALB/c mice. Researchers found that exposure to the high dose resulted in impaired novel object recognition and a change in the expression of genes associated with glutamate metabolism, suggesting possible dysfunction in the hippocampus of female mice (Win-Shwe et al., 2012). These studies highlight the potential for chronic DE exposure to disrupt brain function, but the extent to which these effects are modified/influenced by sex or metabolic stressors such as high-fat diet (HFD) remains poorly understood. Research is essential to better understand the role of DPM in influencing microglial activation and neuroinflammation responses.

4. Cardiovascular Disease and Familial Hypercholesterolemia

Chronic and acute exposure to DPM is associated with cardiovascular disease and mortality (Health Effects Institute, 2025). However, certain populations have an increased vulnerability and susceptibility to DPM-induced health effects. Life stage, preexisting cardiovascular or respiratory disease, genetic polymorphisms, and low-socioeconomic status have all been identified to increase the risk of health effects connected to PM exposure (Sacks et al., 2010). Familial hypercholesterolemia (FH) is an inherited genetic *low-density lipoprotein receptor* (*LDLR*) mutation that prevents LDL uptake into cells, leading to an accumulation of LDL-cholesterol in blood. LDL is the major cholesterol carrier in the bloodstream, with high levels associated with cardiovascular disease and atherosclerosis (Ishibashi et al., 1994). FH has also been associated with cognitive and behavioral impairments and is considered an early risk factor for dementia (de Oliveira et al., 2024). FH is considered one of the most common genetic disorders in the general populations (Hu et al., 2020).

This susceptible population is additionally at risk of developing diet-related health effects, like metabolic dysfunction (i.e., obesity, insulin resistance, high blood pressure). The prevalence of metabolic syndrome is still steadily increasing globally, due to genetic and environmental factors. For women, the prevalence of metabolic syndrome increased from 14.7% in 2000 to 31% in 2023. For men, prevalence rose from 9% in 2000 to 25.7% in 2023 (Noubiap et al., 2025). Co-exposure to a high-fat diet and DPM may increase their risk of PM-related adverse health effects.

Numerous animal studies have been used to investigate the effects of DE on the cardiovascular and pulmonary systems, in addition to neurological and metabolic outcomes (Reis et al., 2018; Weitekamp et al., 2020). The *Ldlr* knockout mouse model has been extensively used to study atherosclerosis and metabolic dysfunction-associated steatohepatitis (MASH) (de Oliveira et al., 2024) and more recently, to link peripheral metabolic dysfunction with adverse brain effects (de

Oliveira et al., 2024). However, the effects of chronic DE in the Ldlr knockout mouse model, and influences by sex and diet, remain largely unexplored.

Rationale, Hypothesis and Aims

Air pollution is a continuing issue worldwide due to its detrimental impact on morbidity and mortality, causing around 4.2 million premature deaths in 2019 according to the World Health Organization. Traffic is a major contributor to particulate matter (PM) in urban areas. PM has been shown to cause pulmonary and cardiovascular dysfunction through inflammation and oxidative stress, with growing research suggesting that PM can also affect the brain and central nervous system. Exposure to PM has been implicated in neurodegeneration, which may result in the development of Alzheimer's disease and related dementias (ADRD). However, the specific molecular mechanisms by which PM exposure contributes to ADRD are not well understood. Microglia, the brain's resident innate immune cells, undergo phenotypic changes in response to pathological conditions that lead to neuroinflammation and disease escalation. However, the microglial phenotypic changes induced by environmental exposures, such as air pollution, remain largely unknown.

The goal of this project is to elucidate neuroinflammatory effects of air pollution, focusing on microglial states. Based on publications and our laboratory's preliminary data, we **hypothesize** that chronic DE exposure will induce sex-specific changes in microglial states and protein pathways, particularly in the hippocampus and olfactory bulb, and that these changes will be exacerbated by HFD in hypercholesterolemic mice. Male and female *low-density lipoprotein receptor* knockout (*Ldlr -/-*) mice, which model FH, a risk factor for dementia, will be exposed to DE or filtered air for 18 weeks, and brains will be collected at the end of the exposures. Using immunohistochemistry (IHC) and proteomics techniques, we will visualize microglial changes

using Iba1, and and proteomic changes due to diet (standard chow vs HFD chow) and DE exposure (DE vs FA) in male and female mice.

Aim 1: Quantify microglial activation induced by diesel exhaust and/or diet exposure in the hippocampus of male and female mice using **immunofluorescence**

Hypothesis: Chronic diesel exhaust exposure induces sex-specific alterations in hippocampal microglial activation, which are modified by high-fat diet

Aim 2: Isolate and characterize the proteomic composition of DE-induced microglial sub-populations in selected brain regions by **isolating protein from mice exposed to filtered air (FA) and diesel exhaust (DE)**

Hypothesis: Chronic diesel exhaust and high-fat diet exposures lead to distinct, sex-specific proteomic alterations in the hippocampus and olfactory bulb associated with neuroinflammation and neurodegeneration

This thesis will establish a mechanistic link between diesel exhaust and diesel particulate matter with neuroinflammation and neurodegeneration, informing public health policies and future studies on particulate matter induced neurological conditions.

Article

1 Introduction

Air pollution affects public health, with about 140 million people in the US alone living in areas with pollution levels above the primary National Ambient Air Quality Standards (NAAQS) (US Environmental Protection Agency, 2024a). A high mortality risk is well-known to result from exposure to air pollution, resulting in about 6.7 million premature deaths annually and ranking as the second leading risk factor for early death worldwide in 2021 (Health Effects Institute, 2024; World Health Organization, 2024). Air pollution exposure is also an important risk factor in cancer, cardiovascular disease, respiratory disease, and reproductive disorders severely affecting low- and middle-income countries, people of racial and ethnic minorities, and those with a low socioeconomic status (Jbaily et al., 2022; NIEHS, 2025; Olloquequi et al., 2024). While air pollution has improved since regulations of the Clean Air Act passed in the 1970s and subsequent amendments, air pollution remains a major public health concern.

Increasing research has raised concern surrounding particulate matter (PM) and its impact on neurodegeneration and psychological well-being. PM can range in size from coarse (PM_{10}) to fine ($PM_{2.5}$) and ultrafine ($PM_{0.1}$;UFP), with inhalation being the primary route of exposure (US Environmental Protection Agency, 2024b). Traffic contributes greatly to urban PM air pollution with diesel engines contributing to a larger particle mass and number than gasoline engines. These particles often adsorb different compounds, like semi-volatile organic compounds (SVOC) and metals, which can produce toxicity effects. The physical particle itself can cause issues, as UFP can be deposited into the lower respiratory space and enter systemic circulation due to their small size. Once in circulation, they can then reach other organs like the brain by crossing the blood-brain barrier (Gerber et al., 2024). Inhaled PM can also enter the brain through the olfactory epithelium, effectively impacting the central nervous system (CNS). Exposure to diesel particulate matter (DPM) has been shown to cause oxidative stress and inflammation leading to neuronal

injury and death. This can ultimately promote neurodegeneration, which is linked to Alzheimer's disease and related dementias (ADRD) (Balachandar et al., 2025; Olloquequi et al., 2024).

Though much research has been done to uncover how DPM contributes to neurodegeneration and aging**,** the specific molecular mechanisms are not well understood. Current research has found that microglia may play an important role in PM-induced neurodegeneration. Microglia are the main innate immune cells in the brain and are key regulators of PM-induced toxicity. To protect the CNS from damage, microglia switch to different states in response to their environment. They are responsible for the phagocytosis and elimination of foreign entities and dead cells and trigger an inflammatory response, among other roles. This inflammation is initially beneficial as it works to maintain homeostasis and repair damage, but continued neuroinflammation can lead to disease pathogenesis. In the case of ADRD, early and continued activation of microglia may be involved in the initiation and progression of the disease, with pro-inflammatory microglia affecting the homeostatic function of microglia, neurons, and astrocytes (Saitgareeva et al., 2020a). Additional research is still needed to understand microglial states and clarify their role in neurodegenerative diseases.

Co-exposure of DPM with other risk factors may increase the risk of developing adverse health effects. Familial hypercholesterolemia (FH) is an inherited genetic *low-density lipoprotein receptor* (*LDLR*) mutation that prevents LDL uptake into the cells. This susceptible population has an increased risk of atherosclerosis and cardiovascular disease (de Oliveira et al., 2024; Hu et al., 2020). They are additionally at risk of developing diet-related health effects, like metabolic dysfunction (i.e., obesity, insulin resistance, high blood pressure). The prevalence of metabolic syndrome is still steadily increasing globally, due to genetic and environmental factors. For women, the prevalence of metabolic syndrome increased from 14.7% in 2000 to 31% in 2023. For men, prevalence rose from 9% in 2000 to 25.7% in 2023 (Noubiap et al., 2025). This mutation is also considered an early risk factor for cognitive decline and dementia (de Oliveira et al., 2024;

Hu et al., 2020). Research into the molecular aspects of PM-induced microglial dysfunction may allow us to further understand its impact on susceptible populations, like those with FH.

Our goal was to characterize the effects of chronic DE exposure, sex, and a high-fat diet (HFD) on neuroinflammatory and proteomic responses in the hippocampus and olfactory bulb of a mouse model of familial hypercholesterolemia. We hypothesize that chronic DE exposure will induce sex-specific changes in microglial states and protein pathways, particularly in the hippocampus and olfactory bulb, and that these changes will be exacerbated by HFD in hypercholesterolemic mice. This hypothesis is based on publications as well as preliminary data indicating that mice exposed chronically to DE develop neuroinflammation and impaired spatial memory (Hullmann et al., 2017b; Li et al., 2020).

2 Methods

2.1 Diesel Exhaust Characterization

Diesel exhaust (DE) characterization has been described in previous publications (Fox et al., 2015; Gould et al., 2008). To mimic the dispersion of DE within the atmosphere, a two-stage dilution system was used, 82% load, with a Yanmar diesel generator (Yanmar model YDG5500EV-6EI). This two-stage dilution system allows for the concentration of DPM to be adjusted and controlled (**Fig.4.**). Ultra-low sulfur diesel fuel (maximum sulfur content 15 ppm) was purchased from local fuel distributors to mimic current highway grade (2) diesel fuel.

Using a micro-orifice uniform deposition impactor (MOUDI) the median aerodynamic diameter was determined, for generated PM, to be 77 nm (UFP). Exposure components of the Yanmar generator yielded average concentrations for elemental carbon (1.03 μg/μg), organic carbon (0.10 μg/μg), particle-bound polycyclic aromatic hydrocarbon (21 ng/μg), nitrogen dioxide (190 ppb), nitric oxide (1160 ppb), carbon dioxide (790 ppm), and carbon monoxide (1.34 ppm) (Fox et al., 2015).

2.2 Animal Husbandry and Diesel Exhaust Exposure

Ldlr knockout (*Ldlr*$^{-/-}$) mice were purchased from The Jackson Laboratories and acclimated to the UW Northlake Diesel facility vivarium for one week. At the start of exposures, mice (*Ldlr -/-*) were 6 weeks old. Mice were exposed to filtered air (FA) and fed a HFD (Male = 13, Female = 13), FA and fed a standard chow diet (Male = 13), DE (~250 µg/m^3) and fed a HFD (Male = 13, Female = 13), or DE and fed a standard chow diet (Male = 13). Over 18 weeks, mice were exposed to FA or DE within their cages (Allentown) for 6 h a day, 5 days per week. This exposure paradigm was used based on previous experiments that found accelerated plaque formation, motor function impairment, and oxidate stress and inflammation (Ehsanifar et al., 2019; Hullmann et al., 2017a).

DE was generated following a previously described protocol (Gould et al., 2008). A diesel generator (Yanmar model YDG5500EV-6EI) with highway-grade number 2 diesel fuel was used. Through a two-stage dilution system, meant to mimic the dispersion of DE in the atmosphere, the concentration of DE was adjusted with FA, creating a concentration of ~250 µm/m^3. Piping directly connected to the DE cage rack was used to uniformly supply cages with DE. The FA cage rack was exposed similarly; FA was pulled through a carbon and HEPA filter and was uniformly released into the FA rack through piping.

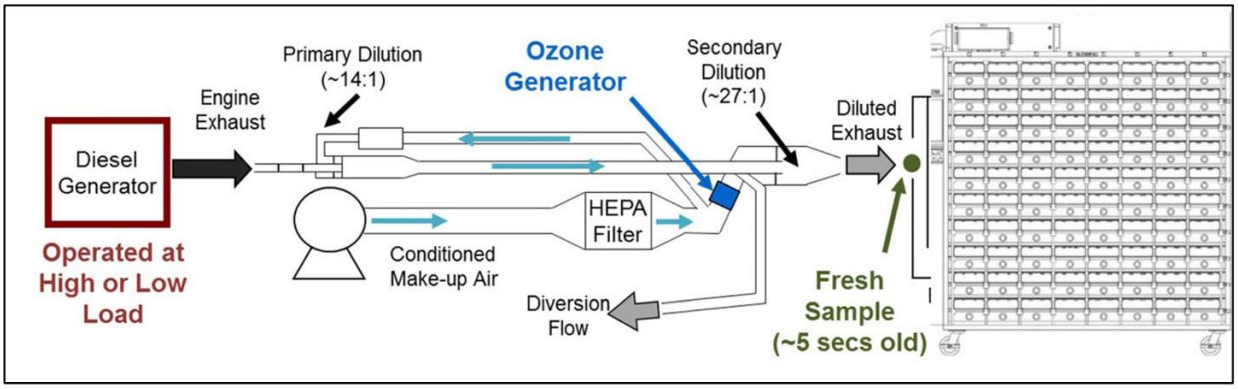

Figure 4. Diesel exhaust exposure schematic adapted in Biorender.com by (Phillips, 2022) from (Fox et al., 2015). This system contains a two-step dilution system that allows for the control of PM concentration.

2.3 Tissue Preparation

At 18 weeks, mice were sacrificed using isoflurane overdose and transcardially perfused with ice cold PBS (1x). The brain was isolated and the right and left hemispheres were separated. To preserve the left hemispheres for immunofluorescence, they were fixed in 4% paraformaldehyde, then placed into a 1x Phosphate Buffered Saline (PBS) + 0.02% NaN_3 (sodium azide) solution. The left hemispheres were then cryoprotected in a 30% sucrose solution for three days, embedded into OCT, and stored at -80°C until cryosectioned. OCT embedded tissues were coronally sectioned at 40 µm and transferred into a 12-well plate with PBS. Prepared plates were stored at 4°C until use. Hippocampal sections were identified using the Allen Mouse Brain Atlas and used for immunofluorescence analysis.

To preserve tissues for proteomics, the hippocampus and olfactory bulb (n = 12-13, per group) were dissected from right hemispheres and flash-frozen in liquid nitrogen. Batch design was randomly balanced based on condition ratios for each tissue type. Condition groups included: male or female, chow or high fat diet, and diesel exposure or filtered air control. An inter-experiment control of samples from a previous pilot assay was created for the hippocampus (pool of 15 samples) and olfactory bulb (pool of 19 samples). Each tissue type was processed separately. Tissues were placed into a lysis buffer (100 mM Tris, 2% SDS, 1x HALT protease and phosphatase inhibitors, and 400 ng/µl enolase) and briefly probe-sonicated on ice. A bicinchoninic acid (BCA) protein assay was performed to determine protein concentration. An inter-batch control was created for the hippocampus (pool of 77 samples) and olfactory bulb (pool of 76 samples).

Each tissue type was prepared in half 96-well plate batches. Batch 1 is 48 samples and controls from row A-D and batch 2 is 48 samples and controls from row E-H. Solutions were prepared for reduction and alkylation by adding lysis buffer and 50 µg of sample into protein LoBind tubes. Enolase (4 ng/µl final) was added into each tube, along with 10 mM TCEP and 15 mM IAA. Protein

was precipitated using 250 µg of MagReSyn Hydroxyl beads (Resyn Biosciences) in a KingFisher Apex (ThermoFisher). Lipids were precipitated using a final concentration of 60% n-Butanol/20% Acetonitrile/20% Water. Then, samples were washed twice with 95% acetonitrile, twice more with 70% ethanol, and then trypsin (1:20 ratio) was added. We used a Kingfisher Apex automated wash/digestion/elute protocol to digest the samples and quenched them with trifluoroacetic acid (0.5% final). Samples were then frozen at -80˚C until mass spectrometry analyses.

2.4 Immunofluorescence

Selected sections (n = 2 per group) were transferred into a new 12-well plate with 1x Tris Buffered Saline (TBS). Sections were washed 3 times with TBS at 5 min, then incubated in blocking solution for 2 h on a shaker at room temperature (TBS, 0.1% Triton X-100, and 5% donkey serum). After blocking, sections were incubated with goat anti Iba1 primary antibody (1:500, Invitrogen CAT # PA5-18039) on a shaker at 4°C overnight. Sections were washed 3x with 1x Tris Buffered Saline and 0.1% Tween 20 (TBS-T) at 5 mins each, then incubated with donkey anti goat AF 488 secondary antibody (1:500, Invitrogen CAT # A-11055) for 2.5 hrs at RT. After 3 final washes with TBS-T, sections were mounted onto superfrost slides (Fisher) with VECTASHIELD antifade mounting medium with DAPI (Vector Laboratories) and a coverslip was placed over the tissue. A 1024 x 1024 Z-stack image (40x) was taken of stained slides using a Nikon A1R HD25 laser scanning confocal microscope.

2.5 Liquid Chromatography and Mass Spectrometry

Peptides were eluted from a PepSep C18 15 cm column with 150 µm inner diameter and 1.9 µm particle size (Bruker), combined with a PepMap C18 5 mm Neo Trap Cartridge with 300 µm inner diameter (Thermo Scientific), and a Fossil Sharp Singularity LOTUS 5 cm hydrophobic coated nESI emitter with 20 µm inner diameter and 363um outer diameter (Fossil Ion Technology). A 50°C heated source (CorSolutions) was used to electrospray two µg of each digested sample with 300 femtomole of Pierce Retention Time Calibrant (PRTC) onto a Thermo Scientific Vanquish

Neo UHPLC system coupled with a Thermo Orbitrap Eclipse Tribrid Mass Spectrometer with the application of a distal 3 kV spray voltage.

The PRTC was used to assess the system suitability of the column and instruments before and during analysis. We analyze system suitability runs prior to any sample analysis and then after every six sample runs another system suitability run is analyzed. Buffer A is 0.1% formic acid in water and buffer B is 0.1% formic acid in 80% acetonitrile.

The 25-minute system suitability gradient consists of a 4 to 6% B in 0.7 minutes, 6 to 6.5% B in 0.3 minutes, 6.5 to 40% B in 20 minutes, 40 to 55% B in 0.5 minutes, followed by a wash of 99% B for 3.5 minutes at a flow rate of 1.3 uL/min. The 60-minute sample LC gradient consists of a 4 to 6% B for 0.7 minutes, 6 to 6.5% B in 0.3 minutes, 6.5 to 40% B in 55.7 minutes, 40 to 55% B in 0.5 minutes, followed by a wash of 99% B for 2.8 minutes at a flow rate of 0.8 to 1.3 uL/min.

For the system suitability analysis, a cycle of one 30,000 resolution full-scan mass spectrum (400-810 m/z) with AGC target of 4e5 and maximum injection time of 50 millisecond (ms) followed by a data-independent acquisition (DIA) MS/MS spectra on a loop count of 20 using an inclusion list of +2 precursor charges at 15,000 resolution, AGC target of 5e4, 22 ms maximum injection time, 30% normalized collision energy with a 2 m/z isolation window.

For the sample digest, first a chromatogram library of 6 independent 60 minute injections is analyzed from a pool of all samples within a batch. For each injection a cycle of one 30,000 resolution full-scan mass spectrum with AGC target of 4e5 and maximum injection time of 50 ms and a mass range of 110 m/z (395-505 m/z, 495-605 m/z, 595-705 m/z, 695-805 m/z, 795-905 m/z, 895-1005 m/z) followed by a DIA MS/MS spectra on a loop count of 25 using an inclusion list of +3 precursor charges at 30,000 resolution, AGC target of 5e5, 54 ms maximum injection time, 27% normalized collision energy with a 4 m/z overlapping isolation window. The chromatogram library data is used to quantify proteins from individual sample runs.

These individual runs consist of a 60 minute cycle of one 30,000 resolution full-scan mass spectrum with a mass range of 350-1005 m/z with AGC target of 4e5 and maximum injection time of 50 ms followed by a DIA MS/MS spectra on a loop count of 75 using an inclusion list of +3 precursor charges at 30,000 resolution, AGC target of 4e5, 54 ms maximum injection time, 27% normalized collision energy with an overlapping 12 m/z isolation window. Application of the mass spectrometer and LC solvent gradients are controlled by the ThermoFisher Xcalibur data system.

2.6 Data-independent acquisition (DIA) signal processing

System suitability runs and process controls were analyzed using Skyline (MacLean et al., 2010) and AutoQC via PanoramaWeb (Bereman et al., 2012; Sharma et al., 2014). Sample raw files were processed by these automated Nextflow workflows (Di Tommaso et al., 2017): 1) https://github.com/mriffle/nf-carafe-ai-ms, git revision: e6eab37fd6, 2) https://github.com/nf-teirex-dia, git revision: 90a4fc3b67 and 3) https://github.com/mriffle/nf-dia-batch-correction, git revision: d79b6e2b5b. The details of the processing within the nextflow workflows are as follows - Thermo XCalibur RAW files were converted to mzML format using Proteowizard using vendor peak picking and demultiplexing ((Amodei et al., 2019; Egertson et al., 2013) with the settings of “overlap_only” and Mass Error = 10.0 ppm. On column chromatogram libraries were created using the data from the six gas phase fractionated “narrow window” DIA runs of the pool from the 66 or 67 samples. These narrow windows were analyzed using EncyclopeDIA (Pino et al., 2020; Searle et al., 2018; Ting et al., 2017) with the default settings (10 ppm tolerances, trypsin digestion, HCD b- and y-ions) with a Carafe (Wen et al., 2025) fine-tuned spectral library from a control pooled sample based on the Uniprot mouse canonical FASTA. The results from this analysis were saved as a “Chromatogram Library" in EncyclopeDIA’s eLib format. The “wide window” DIA runs were analyzed using EncyclopeDIA requiring a minimum of 3 quantitative ions and filtering peptides with q-value ≤ 0.01 using Percolator 3.01. After analyzing each file individually, EncyclopeDIA was used to generate a “Quant Report" which stores all the detected peptides, integration boundaries,

quantitative transitions, and statistical metrics from all runs in an eLib format. The Quant Report eLib library was imported into Skyline with the mouse Uniprot FASTA as the background proteome to map peptides to proteins, perform peak integration, manual evaluation, and report generation. Two separate Skyline documents were created. In one document proteins were associated into groups based in which peptides were mapped to all potential proteins and therefore this document will have duplicated proteins. The second Skyline document contains unique peptides associated with the protein group with the most peptides only. A tsv file of peptide level total area fragments (TAFs) for each replicate was exported from Skyline using the custom reporting capabilities of the document grid for both the duplicated and unique Skyline document. Peptide quantities were then median normalized and batch corrected using ComBat. Principal component analysis was used to check if there were any batch effects based on acquisition number, batch, sex, and treatment. The Skyline documents, raw files and all other associated files for DIA library generation and DIA sample analysis are available at Panorama Public.

2.7 Peptide Data Analysis

Proteomics data were log transformed and then scale normalized to have the same median. The normalized data were then analyzed using the Bioconductor limma package (Ritchie et al., 2015), which has broad applicability to high-throughput data. Group means were computed and then compared using empirical Bayes adjusted contrasts after de-trending the mean-variance relationship (Ritchie et al., 2015). Briefly, the limma package estimates a variance hyperparameter based on all the proteins which is used as a prior to adjust the sample variance for each protein when making comparisons between groups. Even after log transformation there remains a dependence between the mean protein abundance and the estimated variance. The limma-trend pipeline estimates the trend between the mean and variance and de-trends the residuals prior to computing contrasts. The p-values were adjusted for multiple comparisons using false discovery

rate (FDR), and proteins were considered to have significantly differential abundance at an FDR<0.05 (Benjamini & Hochberg, 1995).

2.8 Cell Count and Soma and Arborization Area Measurements

Soma and arborization area measurements were made following a previously described protocol (Ibanez et al., 2019). For each group (**Table 1**), two replicate images were taken at 40x. An additional 40x image (3x zoom, 1024 x 1024) was taken for each group, where three random microglia were selected for measurement in FIJI. A total of 6 recorded measurements for each condition were taken and then averaged. The chow DEM group contained only 3 recorded measurements, as one image was taken using the wrong pixel size, 512 x 512, and therefore could not be compared to the other images. The freehand tool was used to draw a rough circle around the soma body, then a brush tool was used to create a more precise perimeter. The polygon selection tool was used to create a perimeter around the microglia by clicking at the tips of the microglial branches (**Fig.5.**).

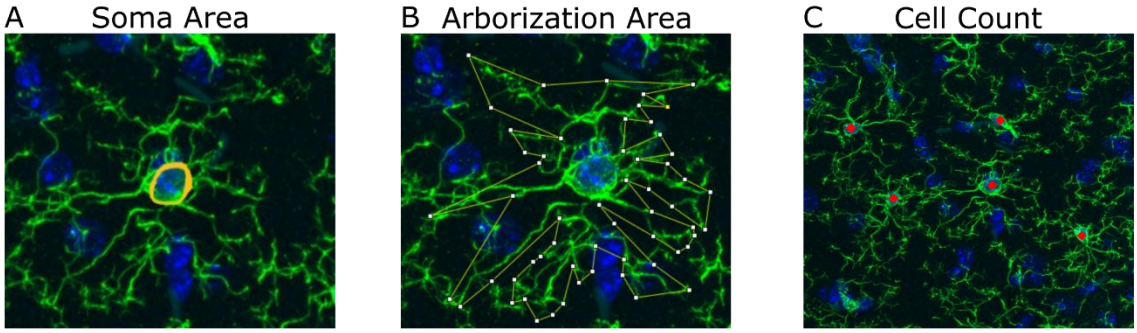

Figure 5. Cell measurements were made for the (A) soma (μm^2) and (B) arborization area (μm^2) of 3 randomly chosen microglia in the 40x (3x zoom) image, for all groups (n = 1, 2 replicates). A cell count was done on 40x images taken for each group (n = 1, 2 replicates). Measurements for the chow DEM group are from one replicate.

Using the multi-point tool in FIJI, diamonds were placed over cells that expressed both Iba1 and Dapi (fig.5C.) The total dual stained cells were summed for each 40x image and the average was taken. For the males, cell count change (%) was calculated by subtracting averaged cell counts by the average cell count of chow FAM, dividing by the average cell count of chow FAM, and multiplying by a hundred. For the females, cell count change (%) was calculated by subtracting average cell count by the average cell count of HFD FAF, dividing by the average cell count of HFD FAF, and multiplying by a hundred. An additional cell count change (%) was calculated for the summed DE group (chow DEM, HFD DEM, HFD DEF) when compared to the summed FA group (chow FAM, HFD FAM, HFD, FAF), to determine if changes we see based on sex remain the same.

Sex	Diet	Exposure	Abbreviated Name
Male	standard chow	Filtered Air (FA)	chow FAM
Male	standard chow	Diesel Exhaust (DE)	chow DEM
Male	HFD chow	Filtered Air (FA)	HFD FAM
Male	HFD chow	Diesel Exhaust (DE)	HFD DEM
Female	HFD chow	Filtered Air (FA)	HFD FAF
Female	HFD chow	Diesel Exhaust (DE)	HFD DEF

Table 1. List of groups and their abbreviated names, used within this study.

2.9 Statistics

All statistical analyses for soma and arborization averages, and cell count were performed using R studio cloud (Posit, 2025). Before linear regression, a shapiro-Wilk test was used to test data normality. To determine statistical significance based on diet, sex, and exposure (DE or FA) linear regressions (ANOVA III) were conducted. Estimated marginal means posthoc tests with Tukey adjustment were used to compare means. A confidence interval of 95% was used for all statistical tests.

3 Results

3.1 Cell Count

Cell counts were quantified from 40x confocal images (**Fig. 5**). Average cell counts and % change was quantified for control and exposed groups (**Fig. 5**). A significant decrease (42%, $p = 0.0463$) in microglia was found in the HFD DEF group, when compared to the HFD FAF group (**Fig. 6**). Compared to the control (chow FAM), a 9% decrease in identified microglia was found for the chow DEM group, a 28% increase for the HFD FAM group, and 13% increase for the HFD DEM group. A 12% decrease in microglia was found in the HFD DEM group when compared to the HFD FAM group. An overall decrease (26%) in microglia was found in the DE groups when compared to the FA groups ($p = 0.0521$; **Fig. 6**).

A

	Cell Count Ave ± SD	% Change
chow FAM	32 ± 2.121	**100%**
chow DEM	29	((29-32)/32)*100 = **-9.375%**
HFD FAM	41 ± 3.536	((41-32)/32)*100 = **28.125%**
HFD DEM	36 ± 12.728	((36-32)/32)*100 = **12.500%**
HFD FAF	69 ± 2.121	**100%**
HFD DEF	40 ± 2.828	(40/69) *100 = **-42.029%**
FA	47 ± 19.296	**100%**
DE	29 ± 5.568	((35-47)/47)*100 = **-25.532%**

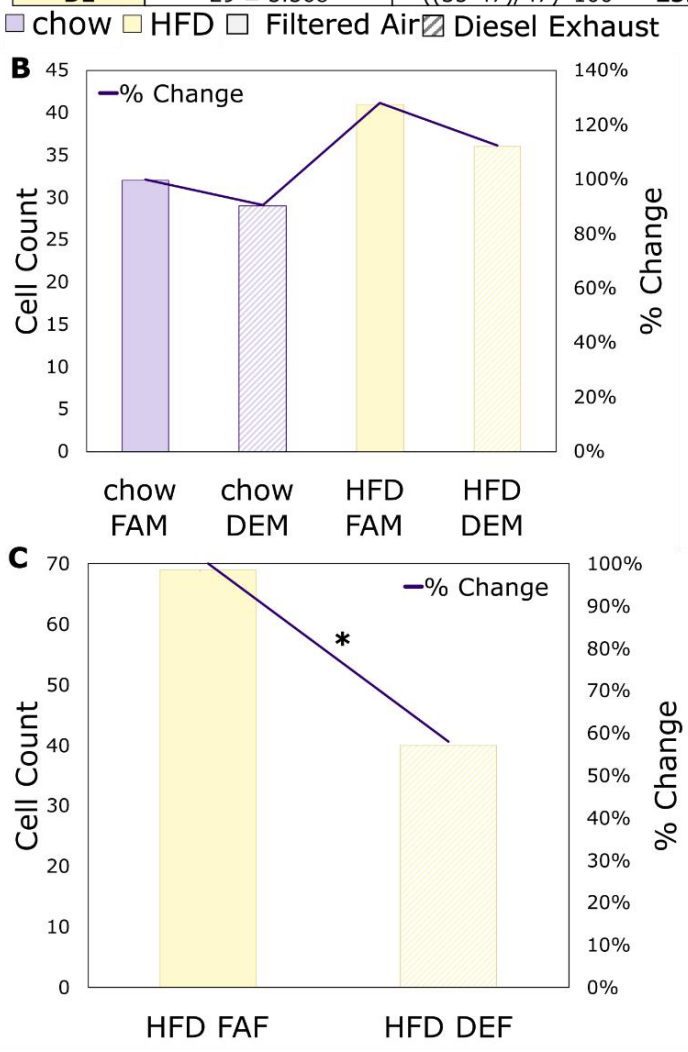

Figure 6. (A) Table comparing cell count average and % change. (B) Cell count comparison (%) between male control (chow FAM) and exposed male groups (chow DEM, HFD FAM, and HFD DEM. No significant changes in cell count were found between controls and exposed, but compared to the control (chow FAM), an 8% decrease in identified microglia was found for the chow DEM group, a 29% increase for the HFD FAM group, and 14% increase for the HFD DEM group. In graph (C) a comparison between the female control, HFD FAF, and exposed, HFD DEF, conveyed a significant decrease (42%, $p = 0.01$). in cell count in the HFD FAF group. Asterisks (*) indicate statistically significant changes from controls ($p < 0.05$).

3.2 Microglial Soma and Arborization Area

Soma and arborization areas were quantified for control and exposed groups (**Table 2**). An increase in soma (~19%) and arborization area (~66%) was found when comparing the HFD FAF and HFD DEF groups. An increase in arborization area (~29%) and decrease in soma area (~5%) was found when comparing the chow FAM and chow DEM groups. A decrease in soma (~9%) and arborization area (~6%) was found when comparing the HFD FAM and HFD DEM groups. When comparing all FA groups against DE groups, an increase in soma (~2%; p = 0.204) and arborization area (~28%; $p = 0.64$) is found, though there is no significant effect.

A

Soma Area (μm²)	Arborization Area (μm²)	Soma Area (μm²)	Arborization Area (μm²)
chow FAM		chow DEM	
36.37 ± 8.792	941.967 ±361.986	34.728 ± 8.734	1216.459 ± 741.647
HFD FAM		HFD DEM	
35.984 ± 12.151	874.971 ± 328.025	32.91 ± 10.790	826.066 ± 725.094
HFD FAF		HFD DEF	
36.077 ± 9.404	715.953 ± 111.911	42.828 ± 8.903	1191.162 ± 468.331
FA		DE	
36.144 ± 9.602	844.297 ± 288.761	36.822 ± 9.299	1077.896 ± 528.740

B

Up	1%-10%	11%-20%	21%-49%	50%+

Down	1%-10%	11%-20%	21%-49%	50%+

	Soma Area (%)	Arborization Area (%)
chow FAM vs chow DEM	**-4.515**	**29.140**
chow FAM vs HFD FAM	**-1.061**	**-7.112**
chow FAM vs HFD DEM	**-9.513**	**-9.513**
HFD FAM vs HFD DEM	**-8.543**	**-5.589**
HFD FAF vs HFD DEF	**18.713**	**66.374**
FA vs DE	**1.877**	**27.668**

Table 2. (A) Average soma and arborization areas (μm^2) calculated by averaging the measurements taken for each group (n = 6, n = 3 for chow DEM). Male exposure groups were compared to the male control (chow FAM), while females were compared to HFD FAF A comparison was also made between the HFD FAM and HFD DEM groups. (B) Percent changes were calculated for each group by subtracting the exposed group from the control (chow FAM or HFD FAF), dividing by the control, then multiplying by 100. Increases are positive and highlighted with a yellow to brown color, while decreases are negative and highlighted by a light blue to dark blue color.

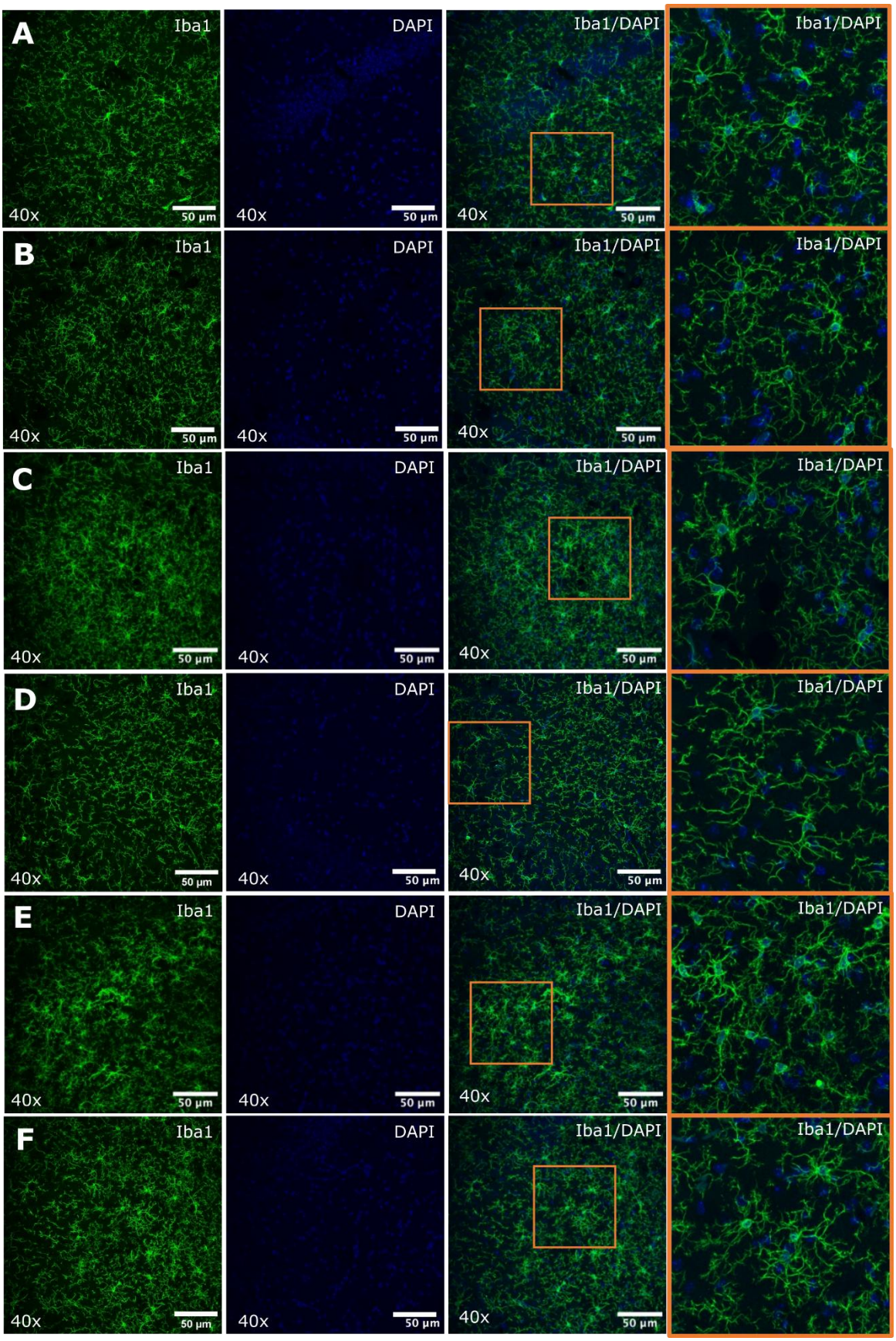
A
Iba1
DAPI
Iba1/DAPI
Iba1/DAPI
40x
50 µm
B
C
D
E
F

Figure 7. Confocal microscopy images (40x, 1024 x 1024) were taken for (A) chow FAM, (B) chow DEM, (C) HFD FAM, (D) HFD DEM, (E) HFD FAF, and (F) HFD DEF brains stained with Iba1, green, and DAPI, blue. Additionally, 40x overlay and 40x, 3x zoom overlay, images were also taken for each group.

3.3 Protein Expression

DIA was used to examine changes in protein expression in the hippocampus and olfactory bulb of mice exposed to DE or FA and fed a HFD or chow diet (**Fig. 8.**). Significant changes (p<0.05) were found in the hippocampus when comparing the HFD DEM and chow DEM groups and the HFD FAM and chow FAM groups, highlighting an effect based on diet. When comparing the HFD DEM and chow DEM groups, a total of 150 significantly changed proteins were found (p<0.05), and the top 3 significant pathways (p<0.05) were regulation of the actin skeleton, diabetic cardiomyopathy, and Fc gamma R-mediated phagocytosis (**Fig. 9**). In the olfactory bulb, significant changes (p<0.05) were found when comparing the HFD FAM and chow FAM groups, highlighting an effect based on diet in males. Significant changes (p<0.05) were also found when comparing the HFD DEF and HFD FAF groups, highlighting an effect based on exposure in females. When comparing the HFD DEF and HFD FAF groups, a total of 596 significantly changed proteins were found in the olfactory bulb (**Fig. 8F**). The top 3 significant pathways (p<0.05) found when comparing the HFD DEF and HFD FAF groups were glutamatergic synapse, oxytocin signaling pathway, and dilated cardiomyopathy (**Fig. 9**). The top 15 upregulated and downregulated proteins can be found in the supplementary materials (**Supp. Fig. 1**). When comparing the top 15 upregulated and downregulated proteins, the male mouse group comparisons in the hippocampus and the olfactory bulb shared 2 similar proteins, Mtarc2 and Serpina (**Supp. Fig. 1.)**. No similarities were found between groups when comparing the top 15 upregulated proteins

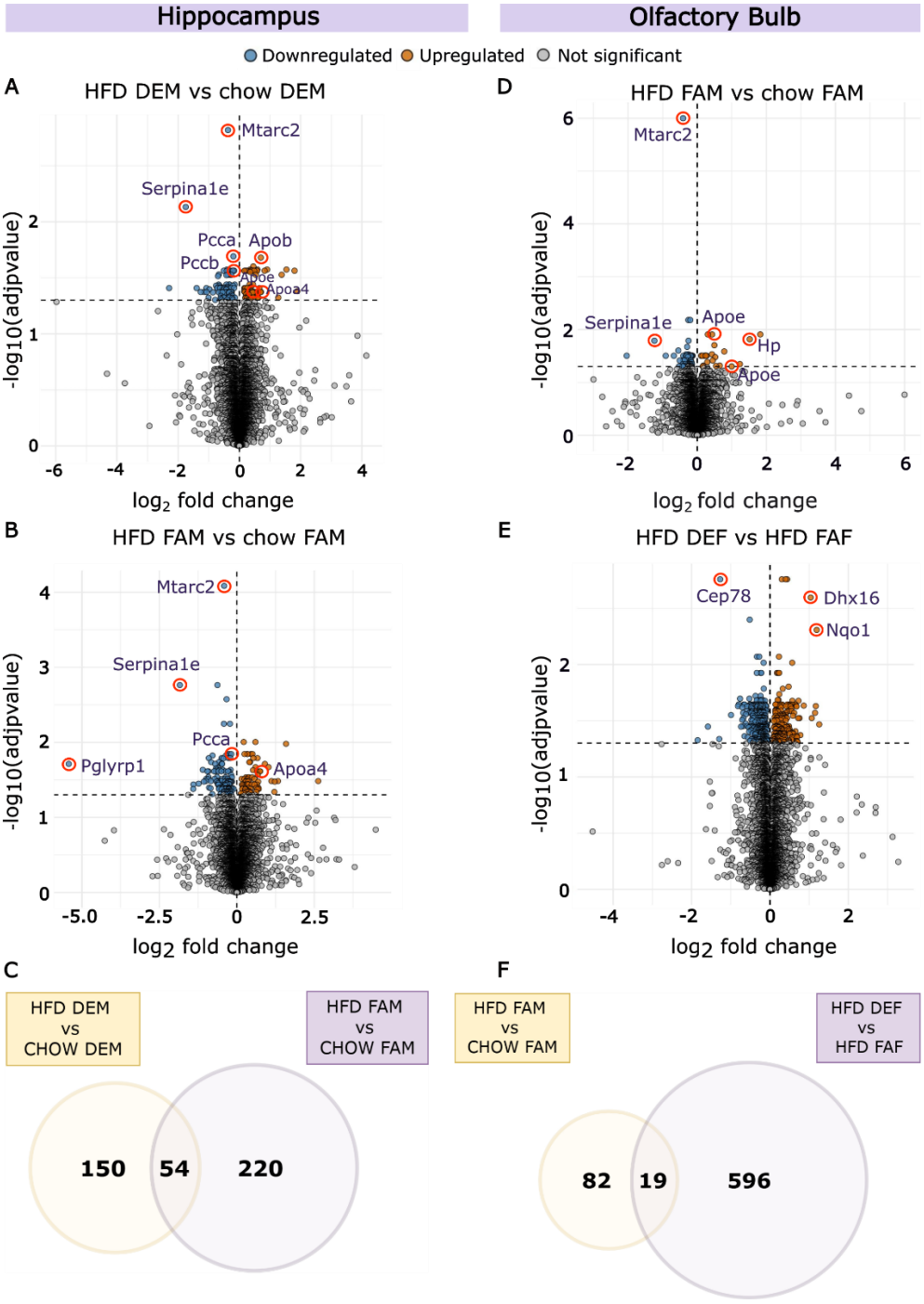

Figure 8. Volcano plots and Venn diagrams outlining the significant protein changes in the hippocampus and olfactory bulb. In the hippocampus, significant changes (p<0.05) were found when comparing between (A) HFD DEM and chow DEM groups and (B) HFD FAM and chow FAM groups. (C) A Venn diagram comparing the two groups within the hippocampus. A total of 54 similarly changed proteins were found between the two. In the olfactory bulb, significant changes (p<0.05) were found when comparing between the (D) HFD FAM and chow FAM groups and the (E) HFD DEF and HFD FAF groups. (F) A total of 19 similarly changed proteins were found between the two groups.

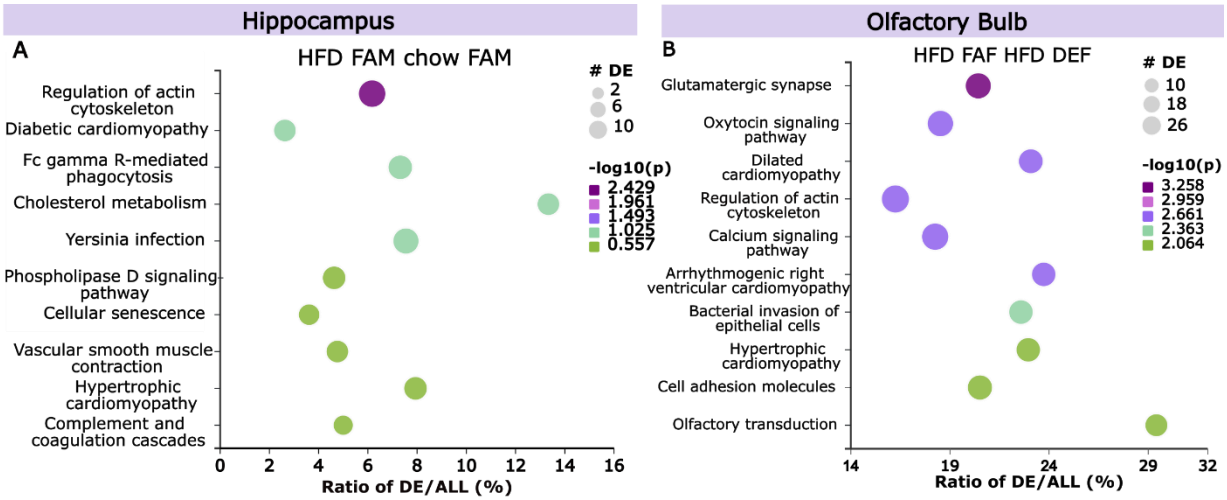

Figure 9. Pathway analysis bubble plots outlining the most significant pathways (p<0.05) changed due to diet and exposure. In the hippocampus, one of the most significant pathways when comparing the (A) HFD FAM and chow FAM groups, was the regulation of the actin cytoskeleton. In the olfactory bulb when comparing the (B) HFD FAF and HFD DEF groups, the most significant pathway was related to glutamatergic synapses.

4 Discussion

With increasing evidence highlighting the heightened risk of neurodegeneration due to diesel exhaust (DE) and ultrafine particulate matter (UFP) exposure, it is important that the specific molecular mechanisms and the contribution of microglia to this process are studied. This study was the first to characterize the sex-dependent effects of chronic DE exposure and diet in the brain of mice (*Ldlr -/-)* susceptible to familial hypercholesterolemia (FH). This study used immunofluorescence to visualize microglia and quantify soma area, arborization area, and microglia cell count. This study also used proteomics to determine protein changes in males and females, based on diet and DE exposure, and determine any changes related to microglia. Overall, the female group fed a HFD and exposed to DE demonstrated possible dysfunction in the olfactory bulb, which may be driving microglial changes we are seeing in the hippocampus, like significant decrease in cell count (adj. p = 0.0463), and an increase in both soma and arborization area. For the male groups, we were unable to determine any driving changes due to DE exposure, but major changes may relate to lipid metabolism dysfunction.

4.1 Microglial Morphology and Number

Microglia are impressive for their ability to repair and protect the brain, and their morphology is often modified depending on changes within the brain. Under noninflammatory conditions, microglia can be found with a small cell body and highly ramified branches, which allows for greater surveillance. During times of stress, microglia will adopt an activated cell morphology that includes the shortening of microglial branches with less ramification and an enlarged cell soma size to aid in movement and phagocytosis (Green & Rowe, 2024).

In our study, trends in arborization area (66% increase) and soma area (19% increase) were found in the HFD DEF group hippocampus when compared to the HFD FAF group. In a few rodent studies, researchers found hyper-ramification of microglia in the hippocampus due to acute and chronic stress (Schramm & Waisman, 2022; Smith et al., 2019). This intermediate state between resting to reactive, is characterized by increased process length, volume, and complexity (Reddaway et al., 2023). Research has shown PM and ozone, which are found in diesel exhaust, to both activate the hypothalamic-pituitary-adrenal axis and trigger the release of stress hormones (Thomson et al., 2013). This has been directly related to effects in the hippocampus of rats, affecting hippocampal volume and impairing memory (Issa et al., 1990; Thomson, 2019). The morphological microglia changes we see in the female group could be attributable to chronic stress due to chronic HFD and DE exposure.

For the male groups an overall decrease in arborization (except chow DEM) and soma area were found in all exposed male groups when compared to the HFD FAM group, highlighting possible microglial activation and phagocytosis (Green & Rowe, 2024). Research on microglial changes dependent on sex often report opposing results related to soma and arborization or ramification. This could be a result of sex-dependent microglial differences during different life stages. For example, some research has found that male rodents have more ameboid, and reactive microglia compared to females in early development (Lenz et al., 2013; Schwarz et al., 2012). Continued

research on the sex differences of microglia may allow us to better understand how our exposures (diet and DE) are affecting microglial morphology and activation.

In addition to morphology, microglial number can be changed with stress. Stress is shown to initially increase proliferation of microglia in stress-responsive brain regions (dentate gyrus, prefrontal cortex, and amygdala) mice, but with chronic stress, proliferation and apoptosis dysfunction leads to a decrease in microglia (Schramm & Waisman, 2022). When assessing microglial quantity in the hippocampus, the combination of DE and HFD in female mice was associated with reduced cell count ($p = 0.0463$). This shift in microglial abundance suggests an elevation of stress within the brain in response to combined environmental and metabolic stressors.

When compared to the chow FAM group, the chow DEM saw a slight decrease in microglial abundance, while the HFD FAM (~28% increase) and HFD DEM (~13% increase) groups saw a slight increase in microglia. The increase in microglial abundance due to DE exposure and HFD is similar to what other studies have found (Cole et al., 2016; Zhuang et al., 2022). The increase in microglia in these groups vs the decrease in the HFD DEF group highlights some possible variability in technique and methods when looking at other studies. The mouse model used may also explain differing results. In a study looking at the effect of diet on the *Ldlr -/-* mouse model, researchers found that a western diet reduced microglial activation, and impaired microglial-driven plaque compaction in Ldlr -/- mice (Kaye et al., 2025). This study is the first to assess the additive effects of diet and DE exposure on the familial hypercholesterolemia, *Ldlr -/-* mouse model, and specific sex-differences in the brain. Continued research is needed to understand the effects diet and DE may have on the brain of Ldlr -/- mice and their specific microglial characteristics.

Variability in technique may have also caused discrepancies in results. When choosing microglia, selection was not consistent to a specific hippocampal region in the brain. Microglial density and stress-responsiveness is greatly dependent on brain region. For example, in the hippocampus,

the CA3 region has a lower microglial density than the CA1 and dentate gyrus (Tan et al., 2020). Our future studies may benefit from standardizing microglial selection and comparing brain regions in males and females.

The main effect of sex on cell count ($f(1,7) = 6.201$, $p = 0.0415$) where our female groups overall had more microglia when compared to males, could be due to biological sex differences in microglial abundance. In a study in rodents, researchers found that in adulthood, microglia showed sex divergence in gene expression, potentially being modulated by male and female hormones (Hanamsagar et al., 2017; Kodama & Gan, 2019). Adult female rodents were also shown to have more microglia in the hippocampus and prefrontal cortex compared to males (Zhang et al., 2025). Developmental stage should be accounted for during exposures as microglial sex differences may mask the true effects of the experimental exposure.

4.2 Sex differences in Protein Expression Changes Based on Diet and Diesel Exhaust Exposure

An overall diet effect on protein expression was seen in the hippocampus of our male groups. Assessment of significantly changed proteins in the hippocampus (**Supp.table.1.**). of the HFD DEM group as compared to the chow DEM group, found significant downregulation of propionyl-CoA carboxylase alpha chain (Pcca) and Propionyl-CoA carboxylase beta chain (Pccb) two proteins associated with propionic acidemia (Ugarte et al., 1999), and significant upregulation of apolipoproteins (Apob, Apoe, Apoa4), and protein tyrosine phosphatases (Pttp) associated with hyperlipoproteinemia type IIa and dyslipidemias (Reijnders et al., 2024). In the olfactory bulb, the HFD FAM group also had a significant upregulation of Apob and Apoe, along with haptoglobin (Hp), when compared to the chow FAM group.

Apolipoproteins are essential to lipid metabolism and dysfunction can have widespread implications. Apoe has been identified as a significant risk factor for late-onset Alzheimer's Disease and certain isoforms have been reported to function in Aβ-dependent and Aβ-independent pathways depending on the Apoe isoform (Islam et al., 2025). Lipid metabolism may

have important implications in neurodegeneration, but the specific mechanisms are not well understood. Continued research on the impact of their dysfunction is needed.

In the olfactory bulb proteomics assessment, one of the top pathways changed when comparing the HFD FAF and HFD DEF groups dealt with the glutamatergic synapse. Glutamatergic synapses mediate synaptic transmission within the CNS (Basilico et al., 2022). In a study that conducted a chronic DPM (100 $\mu g/m^3$) exposure on C57BL/6 mice for 5h per day for 8 weeks, found significantly decreased postsynaptic proteins and N-methyl-D-aspartate (NMDA) receptor subunits (Godoy-Lugo et al., 2025). NMDA is a glutamate receptor and is important to synaptic plasticity (Jewett & Thapa, 2022), while postsynaptic proteins assist with receiving and processing incoming chemical signals (Kalman et al., 2022). These changes suggest DPM can cellularly alter glutamatergic synapses and cause synaptic dysfunction. There is limited research on glutamatergic synapse dysregulation in the olfactory bulb, but glutamatergic signaling dysregulation is often associated with neurodegenerative disorders like Alzheimer's Disease and epilepsy (Pinky et al., 2023). Long-term UFP exposure is linked to olfactory decline in adults between 57-85 years old and is often an early stage of Alzheimer's Disease (Ajmani, Suh, Wroblewski, et al., 2016). More research is needed to uncover the role of glutamatergic synapses in the olfactory bulb and why changes seem to be sex dependent.

Though we did not enrich for microglia in the bulk proteomics data, microglia and glutamatergic synapses hold an interesting relationship. In a study looking at the function of microglia in the regulation of synaptic development and plasticity in the mouse brain, researchers found microglial depletion to harm glutamatergic synapses in adult mice and impair recognition learning. They also assessed the impact of microglial repopulation and found that it rescued negative effects in structure, function, and behavior (Basilico et al., 2022). These findings emphasize the importance microglia play in glutamatergic synapse maintenance and how microglial dysfunction may affect brain health. In another study, researchers assessed the role of macrophage glutaminase (GLS).

GLS is an enzyme, key in the breakdown of glutamine to glutamate. This enzyme has also been thought to play an important part in CNS disorders and $PM_{2.5}$ induced neurotoxicity, by generating excitotoxic glutamate. Researchers found that reactive oxygen species were generated and microglia were activated due to PM introduction, causing oxidative stress. Extracellular vesicles released by olfactory bulb microglia upregulated glutamate production via GLS1, a GLS isoform, contributing to PM2.5-induced neurotoxicity. (Chen et al., 2020). These findings suggest an important role olfactory dysfunction can have on neurological diseases. More research is needed to understand the molecular mechanisms of this pathway.

A notable significantly upregulated ($p = 0.0049$) enzyme found when comparing the HFD FAF and HFD DEF groups was NAD(P)H dehydrogenase, quinone 1 or Nqo1 ($p = 0.0049$). This enzyme is involved in cellular detoxification and protection against oxidative stress (Siegel & Ross, 2000) (Li et al., 2022)and is responsible for the regulation of specific pro-inflammatory cytokines and activation of immune cells in the CNS such as microglia and astrocytes (Li et al., 2022). Research has identified Nqo1 as a possible player in the pathophysiology of acute and chronic neurological disorders, like AD, Parkinson's disease, and traumatic brain injury, in both upregulation and downregulation of Nqo1 (Consortium, 2025). An increase in Nqo1 may highlight an increase in oxidative stress due to DPM exposure.

In the hippocampus proteomics assessment, one of the top pathways changed when comparing the HFD FAM and chow FAM groups was the regulation of the actin cytoskeleton. A study by Hansson et al., demonstrated that remodeling of the actin cytoskeleton correlated to changes in adipocyte size due to a HFD, which impaired insulin sensitivity and glucose tolerance (Hansson et al., 2019). In Alzheimer's disease, synaptic dysfunction is often linked to actin cytoskeleton dysregulation (Tuli et al., 2026). This may suggest that diet is an important modulator to the actin cytoskeleton, which may lead to possible neurological disorders through synaptic dysfunction.

5 Conclusion

Overall, the findings in this project suggest that chronic DE exposure and HFD alter microglial morphology and abundance in a sex-dependent manner, with significant protein changes in pathways relevant to neurodegenerative processes. Additional research is underway and needed to ascertain whether DE-induced microglial states overlap with microglial signatures implicated in Alzheimer's disease and other neurodegenerative conditions, which could provide a mechanistic insight into how air pollution contributes to neurodegenerative disease risk.

Supplementary Figures

Supplementary Table 1. The top 15 upregulated and downregulated proteins in the hippocampus and olfactory bulb

Hippocampus

HFD FAM vs chow FAM

Upregulated				**Downregulated**			
symbol	entrez	logfc	adjpv	symbol	entrez	logfc	adjpv
Alad	17025	0.221	0.010	Mtarc2	67247	-0.411	8E-05
Nptx2	53324	0.600	0.010	Hsd11b1	15483	-0.627	0.002
Ighm	16019	1.588	0.010	Serpina1e	20704	-1.84	0.002
Heatr1	217995	0.454	0.014	Sptb	20741	-0.331	0.003
Gosr2	56494	0.328	0.014	Acbd6	72482	-0.223	0.006
Mrpl45	67036	0.247	0.014	Sms	20603	-0.418	0.006
Rnf181	66510	0.346	0.014	Kbtbd11	74901	-0.304	0.014
Stmn1	16765	0.504	0.014	Pcca	110821	-0.18	0.014
Asic2	11418	0.664	0.016	Thtpa	105663	-0.242	0.014
Cntn6	53870	0.532	0.016	Arhgef6	73341	-0.786	0.015
Trerf1	224829	0.426	0.018	Peak1	244895	-0.355	0.015
Znrf1	170737	0.405	0.018	Arhgef17	207212	-0.493	0.016
Kcna5	16493	0.905	0.019	Dock9	105445	-0.274	0.016
Igkv6-15	108022	1.021	0.021	Pdk3	236900	-0.212	0.016
Kcna6	16494	0.602	0.021	Ribc2	67747	-0.906	0.016

HFD DEM vs chow DEM

Upregulated				**Downregulated**			
symbol	entrez	logfc	adjpv	symbol	entrez	logfc	adjpv
Apob	238055	0.7	0.0209	Mtarc2	67247	-0.372	0.0015
Serac1	321007	0.4553	0.025	Serpina1e	20704	-1.753	0.0074
Col4a3	12828	1.5371	0.0267	Pcca	110821	-0.196	0.0203
Itgb3	16416	0.5875	0.0267	Scrg1	20284	-0.4	0.0267
Stxbp1	20910	0.3507	0.0267	Capzb	12345	-0.336	0.0273
Rgs6	50779	0.9047	0.0267	Nampt	59027	-0.213	0.0273
Ca11	12348	0.5491	0.0273	Gmpr	66355	-0.508	0.0273
Cdh6	12563	0.8247	0.0273	Pccb	66904	-0.169	0.0273
Pura	19290	0.1795	0.0273	Kbtbd11	74901	-0.296	0.0273
Rpia	19895	0.3549	0.0273	Rab30	75985	-0.363	0.0273
Stmn2	20257	0.4636	0.0273	Pdk3	236900	-0.208	0.0273
Rab11fip5	52055	0.2444	0.0273	Sh3bgrl	56726	-0.408	0.0274
Plin5	66968	1.8012	0.0273	Smad3	17127	-0.673	0.0295
Ca10	72605	0.5764	0.0273	Twf1	19230	-0.294	0.0297
Abtb3	74007	0.3845	0.0273	Acad8	66948	-0.264	0.0297

Olfactory Bulb

HFD FAM vs chow FAM							
Upregulated				**Downregulated**			
symbol	entrez	logfc	adjpv	symbol	entrez	logfc	adjpv
Ankrd13a	68420	0.3086	0.0123	Mtarc2	67247	-0.409	1E-06
Apoe	11816	0.4307	0.0123	Acbd6	72482	-0.201	0.0066
Ighg2c	404711	1.826	0.0123	Cyp51a1	13121	-0.257	0.0066
Hp	15439	1.5193	0.0152	Plppr4	229791	-0.253	0.0162
Rnf220	66743	0.496	0.0198	Serpina1e	20704	-1.238	0.0162
Vim	22352	0.7823	0.0259	Dgkg	110197	-0.292	0.0212
Des	13346	0.4267	0.0294	Thtpa	105663	-0.546	0.0249
Agrn	11603	0.1984	0.0313	Coq7	12850	-0.253	0.0294
Fasn	14104	0.1123	0.0313	Tbc1d22a	223754	-0.315	0.0294
Pdcl3	68833	0.2437	0.0313	Adcy2	210044	-0.198	0.0313
Pdzd2	68070	0.2336	0.0313	Agap2	216439	-0.198	0.0313
Sarm1	237868	0.1481	0.0313	Dlgap2	244310	-0.329	0.0313
Smarca5	93762	0.275	0.0313	Elavl2	15569	-0.267	0.0313
Vwa1	246228	0.2485	0.0313	Farsa	66590	-0.147	0.0313
Neu2	23956	0.5212	0.0332	Gatb	229487	-0.201	0.0313
HFD DEF vs HFD FAF							
Upregulated				**Downregulated**			
symbol	entrez	logfc	adjpv	symbol	entrez	logfc	adjpv
G6pdx	14381	0.3029	0.0017	Cep78	208518	-1.27	0.0017
Lgals3bp	19039	0.4378	0.0017	Anln	68743	-0.517	0.004
Pir	69656	0.398	0.0017	Camkk2	207565	-0.272	0.0085
Dhx16	69192	1.039	0.0025	Hpcal4	170638	-0.332	0.0085
Nqo1	18104	1.1928	0.0049	Tanc2	77097	-0.161	0.0096
Scrib	105782	0.2299	0.0085	Atat1	73242	-0.237	0.0119
Th	21823	0.567	0.0096	Ccar2	219158	-0.22	0.0119
Ap3m1	55946	0.1811	0.0119	Clstn3	232370	-0.335	0.0119
Oxsm	71147	0.2097	0.0119	Stxbp1	20910	-0.157	0.0164
Pgd	110208	0.2357	0.0119	Cap2	67252	-0.37	0.019
Htatip2	53415	0.4765	0.0157	Rras2	66922	-0.238	0.019
Abcc4	239273	0.3275	0.0164	Bicdl2	212733	-0.762	0.0201
Sntb2	20650	0.2383	0.0183	Ca10	72605	-0.525	0.0201
Hadha	97212	0.1956	0.0207	Lancl1	14768	-0.185	0.0207
Itgb1	16412	0.2205	0.0207	Pcdhgc5	93708	-0.199	0.0207

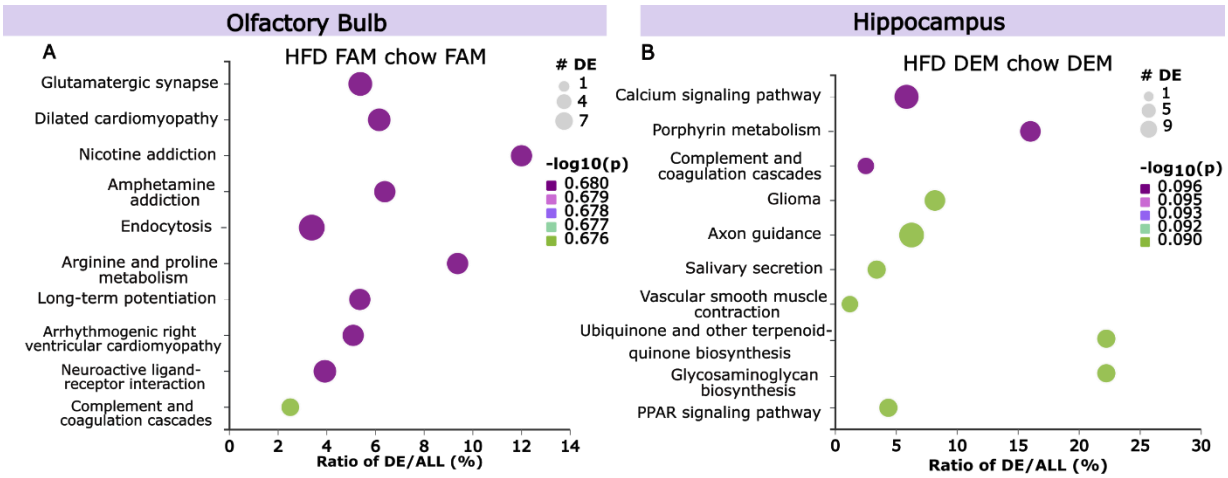

Supplementary Figure 1. Pathway analysis bubble plots did not yield significant results in the olfactory bulb when comparing between the (A) HFD FAM and chow FAM groups and in the hippocampus when comparing the (B) HFD FAF and HFD DEF groups.

Supplementary Table 2. Resulting F and P-values ($\alpha = 0.05$) from comparisons between all main effects, comparisons between male groups, and comparisons between HFD groups. The Adjusted p-values are also listed for comparisons that were trending ($p = 0.05$) or significant ($p < 0.05$).

Main Effects (Cell Count, Soma Area, Arborization Area)						
Group	**Cell Count**		**Soma Area**		**Arborization Area**	
	F(1,7)	P-Value	F(1,7)	P-Value	F(1,7)	P-Value
DE vs FA	5.463	**0.0521**	0.098	0.763	1.543	0.254
HFD vs chow	1.941	0.206	0.156	0.705	0.912	0.372
Female vs Male	6.201	**0.0415***	1.962	0.204	0.235	0.642
Males Only (Cell Count, Soma Area, Arborization Area)						
Group	**Cell Count**		**Soma Area**		**Arborization Area**	
	F(1,3)	P-Value	F(1,3)	P-Value	F(1,3)	P-Value
Male HFD vs Male chow	0.548	0.513	0.0799	0.796	1.556	0.30071
DEM vs FAM	0.0698	0.809	0.0652	0.815	0.769	0.445
Diet x Air Exposure	0.0268	0.8803	0.0297	0.874	0.641	0.482
HFD (Cell Count, Soma Area, Arborization Area)						
Group	**Cell Count**		**Soma Area**		**Arborization Area**	
	F(1,4)	P-Value	F(1,4)	P-Value	F(1,4)	F(1,4)
HFD DE vs HFD FA	17.374	**0.0141***	2.059	0.225	2.222	0.2103
HFD female vs HFD male	0.342	0.59	4.443	0.103	1.312	0.316
Air Exposure x Sex	6.1604	0.068	2.1802	0.214	1.352	0.3096

Cell Count				
	SE	df	t	Adj p value
HFD DEF vs HFD FAF	6.84	4	-4.168	**0.0463***

References

Ajmani, G. S., Suh, H. H., & Pinto, J. M. (2016). Effects of ambient air pollution exposure on olfaction: a review. *Environmental health perspectives*, *124*(11), 1683.

Ajmani, G. S., Suh, H. H., Wroblewski, K. E., Kern, D. W., Schumm, L. P., McClintock, M. K., Yanosky, J. D., & Pinto, J. M. (2016). Fine particulate matter exposure and olfactory dysfunction among urban-dwelling older US adults. *Environmental research*, *151*, 797-803.

Amodei, D., Egertson, J., MacLean, B. X., Johnson, R., Merrihew, G. E., Keller, A., Marsh, D., Vitek, O., Mallick, P., & MacCoss, M. J. (2019). Improving precursor selectivity in data-independent acquisition using overlapping windows. *Journal of The American Society for Mass Spectrometry*, *30*(4), 669-684.

Anand, K. S., & Dhikav, V. (2012). Hippocampus in health and disease: An overview. *Annals of Indian Academy of Neurology*, *15*(4), 239-246.

Bai, N., Kido, T., Suzuki, H., Yang, G., Kavanagh, T. J., Kaufman, J. D., Rosenfeld, M. E., van Breemen, C., & van Eeden, S. F. (2011). Changes in atherosclerotic plaques induced by inhalation of diesel exhaust. *Atherosclerosis*, *216*(2), 299-306.

Balachandar, R., Viramgami, A., Singh, D. P., Kulkarni, N., Chudasama, B., Sivaperumal, P., & Upadhyay, K. (2025). Association between chronic PM2. 5 exposure and neurodegenerative biomarkers in adults from critically polluted area. *BMC Public Health*, *25*(1), 1413.

Barnhill, L. M., Khuansuwan, S., Juarez, D., Murata, H., Araujo, J. A., & Bronstein, J. M. (2020). Diesel exhaust extract exposure induces neuronal toxicity by disrupting autophagy. *Toxicological Sciences*, *176*(1), 193-202.

Basilico, B., Ferrucci, L., Ratano, P., Golia, M. T., Grimaldi, A., Rosito, M., Ferretti, V., Reverte, I., Sanchini, C., & Marrone, M. C. (2022). Microglia control glutamatergic synapses in the adult mouse hippocampus. *Glia*, *70*(1), 173-195.

Benjamini, Y., & Hochberg, Y. (1995). Controlling the false discovery rate: a practical and powerful approach to multiple testing. *Journal of the Royal statistical society: series B (Methodological)*, *57*(1), 289-300.

Bereman, M. S., MacLean, B., Tomazela, D. M., Liebler, D. C., & MacCoss, M. J. (2012). The development of selected reaction monitoring methods for targeted proteomics via empirical refinement. *Proteomics*, *12*(8), 1134-1141.

Bradley, J. M., Cryar, K. A., El Hajj, M. C., El Hajj, E. C., & Gardner, J. D. (2013). Exposure to diesel exhaust particulates induces cardiac dysfunction and remodeling. *Journal of Applied Physiology*, *115*(7), 1099-1106.

Chen, X., Guo, J., Huang, Y., Liu, S., Huang, Y., Zhang, Z., Zhang, F., Lu, Z., Li, F., & Zheng, J. C. (2020). Urban airborne PM2. 5-activated microglia mediate neurotoxicity through glutaminase-containing extracellular vesicles in olfactory bulb. *Environmental Pollution*, *264*, 114716.

Cole, T. B., Coburn, J., Dao, K., Roqué, P., Chang, Y.-C., Kalia, V., Guilarte, T. R., Dziedzic, J., & Costa, L. G. (2016). Sex and genetic differences in the effects of acute diesel exhaust exposure on inflammation and oxidative stress in mouse brain. *Toxicology*, *374*, 1-9.

Consortium, T. U. (2025). UniProt: the Universal Protein Knowledgebase in 2025. *Nucleic acids research*, *53*(D1), D609-D617. https://doi.org/10.1093/nar/gkae1010

Costa, L. G., Cole, T. B., Dao, K., Chang, Y.-C., Coburn, J., & Garrick, J. M. (2020). Effects of air pollution on the nervous system and its possible role in neurodevelopmental and neurodegenerative disorders. *Pharmacology & therapeutics*, *210*, 107523.

Damayanti, S., Harrison, R. M., Pope, F., & Beddows, D. C. (2023). Limited impact of diesel particle filters on road traffic emissions of ultrafine particles. *Environment International*, *174*, 107888.

de Oliveira, J., Moreira, E. L. G., & de Bem, A. F. (2024). Beyond cardiovascular risk: Implications of Familial hypercholesterolemia on cognition and brain function. *Ageing research reviews*, *93*, 102149.

Di Tommaso, P., Chatzou, M., Floden, E. W., Barja, P. P., Palumbo, E., & Notredame, C. (2017). Nextflow enables reproducible computational workflows. *Nature biotechnology*, *35*(4), 316-319.

Egertson, J. D., Kuehn, A., Merrihew, G. E., Bateman, N. W., MacLean, B. X., Ting, Y. S., Canterbury, J. D., Marsh, D. M., Kellmann, M., & Zabrouskov, V. (2013). Multiplexed MS/MS for improved data-independent acquisition. *Nature methods*, *10*(8), 744-746.

Ehsanifar, M., Montazeri, Z., Zavareh, M. S., Rafati, M., & Wang, J. (2023). Cognitive impairment, depressive-like behaviors and hippocampal microglia activation following exposure to air pollution nanoparticles. *Environmental Science and Pollution Research*, *30*(9), 23527-23537.

Ehsanifar, M., Tameh, A. A., Farzadkia, M., Kalantari, R. R., Zavareh, M. S., Nikzaad, H., & Jafari, A. J. (2019). Exposure to nanoscale diesel exhaust particles: Oxidative stress, neuroinflammation, anxiety and depression on adult male mice. *Ecotoxicology and environmental safety*, *168*, 338-347.

Ehsanifar, M., Yavari, Z., & Rafati, M. (2022). Exposure to urban air pollution particulate matter: neurobehavioral alteration and hippocampal inflammation. *Environmental Science and Pollution Research*, *29*(33), 50856-50866.

Fox, J. R., Cox, D. P., Drury, B. E., Gould, T. R., Kavanagh, T. J., Paulsen, M. H., Sheppard, L., Simpson, C. D., Stewart, J. A., & Larson, T. V. (2015). Chemical characterization and in vitro toxicity of diesel exhaust particulate matter generated under varying conditions. *Air Quality, Atmosphere & Health*, *8*(5), 507-519.

Gao, C., Shen, X., Tan, Y., & Chen, S. (2022). Pathogenesis, therapeutic strategies and biomarker development based on “omics” analysis related to microglia in Alzheimer’s disease. *Journal of Neuroinflammation*, *19*(1), 215.

Gerber, L.-S., de Leijer, D. C., Arranz, A. R., Lehmann, J. M., Verheul, M. E., Cassee, F. R., & Westerink, R. H. (2024). In vitro neurotoxicity of particles from diesel and biodiesel fueled engines following direct and simulated inhalation exposure. *Environment International*, *184*, 108481.

Godoy-Lugo, J. A., Hicks, D., Durra, S., Massey, E. R., Shkirkova, K., Sauri, A. I., Kerstiens, E., Chen, S., Zhao, L., & Sioutas, C. (2025). Air pollution decreases postsynaptic PSD-95 and NMDA receptor subunits in synaptosomes from mouse cerebral cortex. *Environmental Pollution*, 126845.

Gould, T., Larson, T., Stewart, J., Kaufman, J. D., Slater, D., & McEwen, N. (2008). A controlled inhalation diesel exhaust exposure facility with dynamic feedback control of PM concentration. *Inhalation toxicology*, *20*(1), 49-52.

Green, T. R., & Rowe, R. K. (2024). Quantifying microglial morphology: an insight into function. *Clinical and experimental immunology*, *216*(3), 221-229.

Hajipour, S., Farbood, Y., Gharib-Naseri, M. K., Goudarzi, G., Rashno, M., Maleki, H., Bakhtiari, N., Nesari, A., Khoshnam, S. E., & Dianat, M. (2020). Exposure to ambient dusty particulate matter impairs spatial memory and hippocampal LTP by increasing brain inflammation and oxidative stress in rats. *Life sciences*, *242*, 117210.

Hanamsagar, R., Alter, M. D., Block, C. S., Sullivan, H., Bolton, J. L., & Bilbo, S. D. (2017). Generation of a microglial developmental index in mice and in humans reveals a sex difference in maturation and immune reactivity. *Glia*, *65*(9), 1504-1520.

Hansson, B., Morén, B., Fryklund, C., Vliex, L., Wasserstrom, S., Albinsson, S., Berger, K., & Stenkula, K. G. (2019). Adipose cell size changes are associated with a drastic actin remodeling. *Scientific Reports*, *9*(1), 12941.

Health Effects Institute. (2024). *State of Global Air 2024*. https://www.stateofglobalair.org/resources/report/state-global-air-report-2024
Health Effects Institute. (2025). *State of Global Air 2025*. https://www.stateofglobalair.org/resources/report/state-global-air-report-2025
Hu, P., Dharmayat, K. I., Stevens, C. A., Sharabiani, M. T., Jones, R. S., Watts, G. F., Genest, J., Ray, K. K., & Vallejo-Vaz, A. J. (2020). Prevalence of familial hypercholesterolemia among the general population and patients with atherosclerotic cardiovascular disease: a systematic review and meta-analysis. *Circulation*, *141*(22), 1742-1759.
Hullmann, M., Albrecht, C., van Berlo, D., Gerlofs-Nijland, M. E., Wahle, T., Boots, A. W., Krutmann, J., Cassee, F. R., Bayer, T. A., & Schins, R. P. (2017a). Diesel engine exhaust accelerates plaque formation in a mouse model of Alzheimer's disease. *Particle and fibre toxicology*, *14*(1), 35.
Hullmann, M., Albrecht, C., van Berlo, D., Gerlofs-Nijland, M. E., Wahle, T., Boots, A. W., Krutmann, J., Cassee, F. R., Bayer, T. A., & Schins, R. P. (2017b). Diesel engine exhaust accelerates plaque formation in a mouse model of Alzheimer's disease. *Particle and fibre toxicology*, *14*, 1-14.
IARC, I. (2012). Diesel engine exhaust carcinogenic. *Press release*(213), 1-2.
Ibanez, F. G., Picard, K., Bordeleau, M., Sharma, K., Bisht, K., & Tremblay, M.-È. (2019). Immunofluorescence staining using IBA1 and TMEM119 for microglial density, morphology and peripheral myeloid cell infiltration analysis in mouse brain. *JoVE (Journal of Visualized Experiments)*(152), e60510.
Ishibashi, S., Herz, J., Burns, D., Hammer, R., Gerard, R., Brown, M., & Goldstein, J. (1994). Low density lipoprotein receptor knockout mouse. *Pathophysiology*, *1*, 363.
Islam, S., Noorani, A., Sun, Y., Michikawa, M., & Zou, K. (2025). Multi-functional role of apolipoprotein E in neurodegenerative diseases. *Frontiers in Aging Neuroscience*, *17*, 1535280.
Issa, A. M., Rowe, W., Gauthier, S., & Meaney, M. J. (1990). Hypothalamic-pituitary-adrenal activity in aged, cognitively impaired and cognitively unimpaired rats. *Journal of Neuroscience*, *10*(10), 3247-3254.
Jbaily, A., Zhou, X., Liu, J., Lee, T.-H., Kamareddine, L., Verguet, S., & Dominici, F. (2022). Air pollution exposure disparities across US population and income groups. *Nature*, *601*(7892), 228-233.
Jewett, B. E., & Thapa, B. (2022). Physiology, NMDA receptor. In *StatPearls [Internet]*. StatPearls Publishing.
Jones, A., Ali, M. U., Mayhew, A., Aryal, K., Correia, R. H., Dash, D., Manis, D. R., Rehman, A., O'Connell, M. E., & Taler, V. (2025). Environmental risk factors for all-cause dementia, Alzheimer's disease dementia, vascular dementia, and mild cognitive impairment: An umbrella review and meta-analysis. *Environmental research*, *270*, 121007.
Kalman, Z. E., Dudola, D., Mészáros, B., Gáspári, Z., & Dobson, L. (2022). PSINDB: the postsynaptic protein–protein interaction database. *Database*, *2022*, baac007.
Kaye, S., Gold, A., Lin, D., Chen, M., Zhu, J., & Gao, J. (2025). Hypercholesterolemia drives microglial dysfunction and weakens response to amyloid plaques. *Experimental Neurology*, *390*, 115272.
Kodama, L., & Gan, L. (2019). Do microglial sex differences contribute to sex differences in neurodegenerative diseases? *Trends in molecular medicine*, *25*(9), 741-749.
Lamptey, R. N., Chaulagain, B., Trivedi, R., Gothwal, A., Layek, B., & Singh, J. (2022). A review of the common neurodegenerative disorders: current therapeutic approaches and the potential role of nanotherapeutics. *International journal of molecular sciences*, *23*(3), 1851.

Landwehr, K. R., Larcombe, A. N., Reid, A., & Mullins, B. J. (2021). Critical review of diesel exhaust exposure health impact research relevant to occupational settings: are we controlling the wrong pollutants? *Exposure and Health*, *13*(2), 141-171.
Lenz, K. M., Nugent, B. M., Haliyur, R., & McCarthy, M. M. (2013). Microglia are essential to masculinization of brain and behavior. *Journal of Neuroscience*, *33*(7), 2761-2772.
Li, R., Zhou, Y., Zhang, S., Li, J., Zheng, Y., & Fan, X. (2022). The natural (poly) phenols as modulators of microglia polarization via TLR4/NF-κB pathway exert anti-inflammatory activity in ischemic stroke. *European journal of pharmacology*, *914*, 174660.
Li, X., Zhang, Y., Li, B., Yang, H., Cui, J., Li, X., Zhang, X., Sun, H., Meng, Q., & Wu, S. (2020). Activation of NLRP3 in microglia exacerbates diesel exhaust particles-induced impairment in learning and memory in mice. *Environment International*, *136*, 105487.
Ma, T., Toumasatos, Z., Tang, T., Durbin, T. D., Johnson, K. C., & Karavalakis, G. (2025). Real-world particle emissions from a modern heavy-duty diesel vehicle during normal operation and DPF regeneration events: impacts on disadvantaged communities. *Environmental Science & Technology*, *59*(1), 699-708.
MacLean, B., Tomazela, D. M., Shulman, N., Chambers, M., Finney, G. L., Frewen, B., Kern, R., Tabb, D. L., Liebler, D. C., & MacCoss, M. J. (2010). Skyline: an open source document editor for creating and analyzing targeted proteomics experiments. *Bioinformatics*, *26*(7), 966-968.
Manisalidis, I., Stavropoulou, E., Stavropoulos, A., & Bezirtzoglou, E. (2020). Environmental and health impacts of air pollution: a review. *Frontiers in public health*, *8*, 14.
Matthaios, V. N., Lawrence, J., Martins, M. A., Ferguson, S. T., Wolfson, J. M., Harrison, R. M., & Koutrakis, P. (2022). Quantifying factors affecting contributions of roadway exhaust and non-exhaust emissions to ambient PM10–2.5 and PM2. 5–0.2 particles. *Science of the total environment*, *835*, 155368.
Miller, M. R., & Newby, D. E. (2020). Air pollution and cardiovascular disease: car sick. *Cardiovascular research*, *116*(2), 279-294.
Mueller, S. G., Schuff, N., Yaffe, K., Madison, C., Miller, B., & Weiner, M. W. (2010). Hippocampal atrophy patterns in mild cognitive impairment and Alzheimer's disease. *Human brain mapping*, *31*(9), 1339-1347.
Ng, P. Y., Zhang, C., Li, H., & Baker, D. J. (2023). Senescent microglia represent a subset of disease-associated microglia in P301S mice. *Journal of Alzheimer's Disease*, *95*(2), 493-507.
NIEHS. (2025). *Air Pollution and Your Health* Retrieved 28 May 2025 from https://www.niehs.nih.gov/health/topics/agents/air-pollution
NIH. (2019). *The Life and Death of a Neuron*. National Institute of Neurological Disorders and Stroke.
Noubiap, J. J., Nansseu, J. R., Nyaga, U. F., Ndoadoumgue, A. L., Ngouo, A. T., Tounouga, D. N., Tianyi, F.-L., Foka, A. J., Lontchi-Yimagou, E., & Nkeck, J. R. (2025). Worldwide trends in metabolic syndrome from 2000 to 2023: a systematic review and modelling analysis. *Nature Communications*.
O'Piela, D. R., Durisek, G. R., Escobar, Y.-N. H., Mackos, A. R., & Wold, L. E. (2022). Particulate matter and Alzheimer's disease: an intimate connection. *Trends in molecular medicine*, *28*(9), 770-780.
Olloquequi, J., Díaz-Peña, R., Verdaguer, E., Ettcheto, M., Auladell, C., & Camins, A. (2024). From inhalation to neurodegeneration: air pollution as a modifiable risk factor for Alzheimer's disease. *International Journal of Molecular Sciences*, *25*(13), 6928.
Phillips, A. R. (2022). *Developmental neurotoxicity of diesel exhaust in a Gclm heterozygous mouse model*. University of Washington.

Pinky, P. D., Pfitzer, J. C., Senfeld, J., Hong, H., Bhattacharya, S., Suppiramaniam, V., Qureshi, I., & Reed, M. N. (2023). Recent insights on glutamatergic dysfunction in Alzheimer's disease and therapeutic implications. *The Neuroscientist*, *29*(4), 461-471.

Pino, L. K., Just, S. C., MacCoss, M. J., & Searle, B. C. (2020). Acquiring and analyzing data independent acquisition proteomics experiments without spectrum libraries. *Molecular & Cellular Proteomics*, *19*(7), 1088-1103.

Posit, T. (2025). RStudio: Integrated Development Environment for R. Posit Software, PBC, Boston, MA. In.

Prater, K. E., Green, K. J., Mamde, S., Sun, W., Cochoit, A., Smith, C. L., Chiou, K. L., Heath, L., Rose, S. E., & Wiley, J. (2023). Human microglia show unique transcriptional changes in Alzheimer's disease. *Nature Aging*, *3*(7), 894-907.

Reddaway, J., Richardson, P. E., Bevan, R. J., Stoneman, J., & Palombo, M. (2023). Microglial morphometric analysis: so many options, so little consistency. *Frontiers in neuroinformatics*, *17*, 1211188.

Reijnders, E., van der Laarse, A., Ruhaak, L. R., & Cobbaert, C. M. (2024). Closing the gaps in patient management of dyslipidemia: stepping into cardiovascular precision diagnostics with apolipoprotein profiling. *Clinical Proteomics*, *21*(1), 19.

Reis, H., Reis, C., Sharip, A., Reis, W., Zhao, Y., Sinclair, R., & Beeson, L. (2018). Diesel exhaust exposure, its multi-system effects, and the effect of new technology diesel exhaust. *Environment International*, *114*, 252-265.

Ritchie, M. E., Phipson, B., Wu, D., Hu, Y., Law, C. W., Shi, W., & Smyth, G. K. (2015). limma powers differential expression analyses for RNA-sequencing and microarray studies. *Nucleic acids research*, *43*(7), e47-e47.

Roqué, P. J., Dao, K., & Costa, L. G. (2016). Microglia mediate diesel exhaust particle-induced cerebellar neuronal toxicity through neuroinflammatory mechanisms. *Neurotoxicology*, *56*, 204-214.

Sacks, J. D., Stanek, L. W., Luben, T. J., Johns, D. O., Buckley, B. J., Brown, J. S., & Ross, M. (2010). Particulate matter–induced health effects: who is susceptible? *Environmental health perspectives*, *119*(4), 446.

Saitgareeva, A. R., Bulygin, K. V., Gareev, I. F., Beylerli, O. A., & Akhmadeeva, L. R. (2020a). The role of microglia in the development of neurodegeneration. *Neurological Sciences*, *41*, 3609-3615.

Saitgareeva, A. R., Bulygin, K. V., Gareev, I. F., Beylerli, O. A., & Akhmadeeva, L. R. (2020b). The role of microglia in the development of neurodegeneration. *Neurological Sciences*, *41*(12), 3609-3615.

Schramm, E., & Waisman, A. (2022). Microglia as central protagonists in the chronic stress response. *Neurology: Neuroimmunology & Neuroinflammation*, *9*(6), e200023.

Schraufnagel, D. E. (2020). The health effects of ultrafine particles. *Experimental & molecular medicine*, *52*(3), 311-317.

Schwarz, J. M., Sholar, P. W., & Bilbo, S. D. (2012). Sex differences in microglial colonization of the developing rat brain. *Journal of neurochemistry*, *120*(6), 948-963.

Searle, B. C., Pino, L. K., Egertson, J. D., Ting, Y. S., Lawrence, R. T., MacLean, B. X., Villén, J., & MacCoss, M. J. (2018). Chromatogram libraries improve peptide detection and quantification by data independent acquisition mass spectrometry. *Nature Communications*, *9*(1), 5128.

Sharma, V., Eckels, J., Taylor, G. K., Shulman, N. J., Stergachis, A. B., Joyner, S. A., Yan, P., Whiteaker, J. R., Halusa, G. N., & Schilling, B. (2014). Panorama: a targeted proteomics knowledge base. *Journal of proteome research*, *13*(9), 4205-4210.

Shkirkova, K., Lamorie-Foote, K., Zhang, N., Li, A., Diaz, A., Liu, Q., Thorwald, M. A., Godoy-Lugo, J. A., Ge, B., & D'Agostino, C. (2022). Neurotoxicity of diesel exhaust particles. *Journal of Alzheimer's Disease*, *89*(4), 1263-1278.

Siegel, D., & Ross, D. (2000). Immunodetection of NAD (P) H: quinone oxidoreductase 1 (NQO1) in human tissues. *Free Radical Biology and Medicine*, *29*(3-4), 246-253.
Singh, N., & Sharma, S. (2025). Molecular and immunological mechanisms associated with diesel exhaust exposure. *Targets*, *3*(2), 14.
Smith, K. L., Kassem, M. S., Clarke, D. J., Kuligowski, M. P., Bedoya-Pérez, M. A., Todd, S. M., Lagopoulos, J., Bennett, M. R., & Arnold, J. C. (2019). Microglial cell hyper-ramification and neuronal dendritic spine loss in the hippocampus and medial prefrontal cortex in a mouse model of PTSD. *Brain, behavior, and immunity*, *80*, 889-899.
Song, J., Han, K., Wang, Y., Qu, R., Liu, Y., Wang, S., Wang, Y., An, Z., Li, J., & Wu, H. (2022). Microglial activation and oxidative stress in PM2. 5-induced neurodegenerative disorders. *Antioxidants*, *11*(8), 1482.
Song, S., Fan, M., Feng, R., & Zhao, H. (2026). Airborne particulate matter and the lung-brain axis: unraveling the neuroinflammatory cascade from alveolar irritation to microglial activation. *Journal of Neuroinflammation*, *23*, 142.
Tan, Y.-L., Yuan, Y., & Tian, L. (2020). Microglial regional heterogeneity and its role in the brain. *Molecular psychiatry*, *25*(2), 351-367.
Tanaka, M., Aoki, Y., Takano, H., Fujitani, Y., Hirano, S., Nakamura, R., Sone, Y., Kiyono, M., Ichinose, T., & Itoh, T. (2013). Effects of exposure to nanoparticle-rich or-depleted diesel exhaust on allergic pathophysiology in the murine lung. *The Journal of toxicological sciences*, *38*(1), 35-48.
Thangavel, P., Park, D., & Lee, Y. C. (2025). Neurotoxic effects of airborne particulate matter: Mechanisms and health implications. *Journal of Biochemical and Molecular Toxicology*, *39*(6), e70322.
Thomson, E. M. (2019). Air pollution, stress, and allostatic load: linking systemic and central nervous system impacts. *Journal of Alzheimer's Disease*, *69*(3), 597-614.
Thomson, E. M., Vladisavljevic, D., Mohottalage, S., Kumarathasan, P., & Vincent, R. (2013). Mapping acute systemic effects of inhaled particulate matter and ozone: multiorgan gene expression and glucocorticoid activity. *Toxicological Sciences*, *135*(1), 169-181.
Ting, Y. S., Egertson, J. D., Bollinger, J. G., Searle, B. C., Payne, S. H., Noble, W. S., & MacCoss, M. J. (2017). PECAN: library-free peptide detection for data-independent acquisition tandem mass spectrometry data. *Nature methods*, *14*(9), 903-908.
Tsakonas, G., Stamatiou, R., Vouitsis, I., Sainidis, C., Facio, A. T. J., Introna, M., Steimer, S., Elihn, K., Besis, A., & Kouras, A. (2025). Diesel particle filter regeneration: Impact on the physicochemical composition and toxicity of diesel exhaust emissions. *Science of the total environment*, *1009*, 181099.
Tuli, S., Patel, P., Shethji, A., & Gau, D. (2026). Mitochondria and the Actin Cytoskeleton in Neurodegeneration. *Cytoskeleton*.
Ugarte, M., Pérez-Cerdá, C., Rodríguez-Pombo, P., Desviat, L. R., Pérez, B., Richard, E., Muro, S., Campeau, E., Ohura, T., & Gravel, R. A. (1999). Overview of mutations in the PCCA and PCCB genes causing propionic acidemia. *Human mutation*, *14*(4), 275-282.
US Environmental Protection Agency. (2024a). *NAAQS Table*. Retrieved 27 May 2025 from https://www.epa.gov/criteria-air-pollutants/naaqs-table
US Environmental Protection Agency. (2024b). *Particulate Matter (PM) Basics*. Retrieved 28 May 2025 from https://www.epa.gov/pm-pollution/particulate-matter-pm-basics#PM
Vaaraslahti, K., Virtanen, A., Ristimäki, J., & Keskinen, J. (2004). Nucleation mode formation in heavy-duty diesel exhaust with and without a particulate filter. *Environmental Science & Technology*, *38*(18), 4884-4890.
Weitekamp, C. A., Kerr, L. B., Dishaw, L., Nichols, J., Lein, M., & Stewart, M. J. (2020). A systematic review of the health effects associated with the inhalation of particle-filtered and whole diesel exhaust. *Inhalation toxicology*, *32*(1), 1-13.

Wen, B., Hsu, C., Shteynberg, D., Zeng, W.-F., Riffle, M., Chang, A., Mudge, M. C., Nunn, B. L., MacLean, B. X., & Berg, M. D. (2025). Carafe enables high quality in silico spectral library generation for data-independent acquisition proteomics. *Nature Communications*, *16*(1), 9815.

Win-Shwe, T.-T., Fujimaki, H., Fujitani, Y., & Hirano, S. (2012). Novel object recognition ability in female mice following exposure to nanoparticle-rich diesel exhaust. *Toxicology and applied pharmacology*, *262*(3), 355-362.

World Health Organization. (2024). *Ambient (Outdoor) Air Pollution*. Retrieved 28 May 2025 from https://www.who.int/news-room/fact-sheets/detail/ambient-(outdoor)-air-quality-and-health

Zhang, A. Y., Elias, E., White, A. G., Jones, L. G., Hamad, T., & Manners, M. T. (2025). Microglia reactivity is brain region and sex specific in the context of chronic stress. *Scientific Reports*, *15*(1), 33285.

Zhao, N., Chen, Z., & Sun, H. (2026). Long-term exposure to ambient particulate matter and its association with Alzheimer's disease: influencing factors and a systematic review with meta-analysis. *Frontiers in Public Health*, *14*, 1757872.

Zhuang, H., Yao, X., Li, H., Li, Q., Yang, C., Wang, C., Xu, D., Xiao, Y., Gao, Y., & Gao, J. (2022). Long-term high-fat diet consumption by mice throughout adulthood induces neurobehavioral alterations and hippocampal neuronal remodeling accompanied by augmented microglial lipid accumulation. *Brain, behavior, and immunity*, *100*, 155-171.